

Damage Analysis of Composite Tapered Beams

Anthony J. Vizzini* and Sung W. Lee†

Department of Aerospace Engineering
University of Maryland
College Park, MD 20742

Abstract

The stress state and the resulting failure mechanisms of composite tapered components are investigated. Finite-element modeling and experimental evidence summarized from previous and present efforts are used to determine the location of the damage initiation, the interaction between the free edge and the taper discontinuities, the effect of realistic geometries, the extent and mode of damage growth, and the ability of simple physical models to explain the occurrence of the interlaminar stress state.

Introduction

In the particular application of a flexbeam in a bearingless rotor, composite materials are of great use for their high strength, high stiffness, superb fatigue characteristics, and damage tolerance. The flexbeam is required to be stiff at the hub and flexible at the blade. This can be done by terminating plies at discrete locations to reduce the stiffness of the beam. This results in a taper.

Taper sections have received much attention by researchers. The loading regime of high quasistatic axial (extension), cyclic spanwise bending (flap), cyclic chordwise bending (lead-lag), and cyclic torsion (twist) loads poses a challenge in design. In addition, the requirement of internal ply terminations of a laminated composite structure under such loads increases the complexity. Many fundamental questions have been raised and answered as the result of the previous and ongoing research efforts to understand the structural integrity of composite flexbeams. Yet much remains uncertain and unanswered.

Half of a typical ply-drop configuration of a tapered specimen modeled and tested is shown in Fig. 1. The plies are dropped in symmetric pairs about the centerline. As a result of the manufacture and cure processes, resin-rich pockets form at the end of the dropped plies. In the tapered region, the load carried by the dropped plies is transferred to the belt and core plies. This load transfer takes place through thin interply resin layers surrounding the ply drops and gives

* Associate Professor, member AHS

† Professor, member AHS

rise to significant interlaminar stresses that promote delamination. These out-of-plane stresses peak at each of the ply drops and at the root of the taper. The interply resin layers are the weak link in the component and, when loaded, will fail first. Fracture of the resin layers will result in delamination in the taper region. This will reduce the bending stiffness of the beam and may lead to catastrophic failure of the component.

Much has been done to understand the failure mechanisms that develop in tapered structures under axial loads. Analytically, the tapered section has been modeled to determine the stress state and the strain-energy release rate of delaminations growing in the tapered section [1–6]. Much of the previous efforts have concentrated on a two-dimensional ideal representation of the geometry of the taper. Both numerically intensive finite-element models and simplified analyses have been attempted.

Experimentally, tapered specimens have been manufactured from graphite-epoxy and glass-epoxy composites and have been tested under uniaxial tension under quasistatic conditions and fatigue. In addition to understanding the failure mechanisms, extensive work has been conducted on increasing the structural integrity of the tapered section. Film adhesive was placed around the dropped plies to strengthen the region about the drop and to modify the load transfer, thus decreasing the interlaminar stress state [7]. As had been seen in flat laminates, this method was successful in certain configurations. Reconfiguration of the ply drop locally by extending one ply of the pair into the resin-rich pocket [8] or by reordering the sequence of drops [9] also increased the structural integrity and altered the failure mechanism.

While much has been gained through the analytical and experimental efforts, there are issues that hinder further understanding of the physical phenomena. The issues addressed in this paper regarding the physical phenomenon of failure are:

1. The location of the onset of damage.
2. The failure mechanism itself.

Additional concerns arise from the assumptions used in the modeling of a tapered structure. Those to be addressed are:

1. The adequacy of two-dimensional models in predicting the stress state at and near the ply drop.
2. The validity of assuming ideal taper geometries.
3. The validity of simplified models to explain the physical phenomena.

Finite Element Model

Much of the analytical results presented in this paper are based on a three-dimensional finite-

element model of the tapered composite beam. This model has been used extensively in previous research [2,7–11]. Sublaminates, plies or portions of plies are modeled by a layer of elements. The numbers of elements in the transverse and longitudinal directions are arbitrary. In addition to the plies, thin interply resin layers are included about the ply drop to be studied to allow for the direct calculation of interlaminar stresses. The state of stress in the tapered specimen is determined by fixing the thick end of the specimen in the longitudinal direction and applying a uniform uniaxial displacement on the thin end. The corresponding reaction forces at the thin end can be used to determine the equivalent force or stress level on the specimen. The interlaminar stresses σ_{zz} , σ_{zx} , and σ_{zy} are determined directly from the average stress state in the elements that make up the interply resin layers and are reported in the local x - z plane for those elements in the tapered section at an angle with respect to the longitudinal axis.

In the present study, a baseline tapered configuration is chosen to consist of 28 plies in the thick end, tapering to 16 plies. The remaining 12 plies are terminated symmetrically at three equally spaced locations. The taper angle is nominally 5.71° , which results in a 10-to-1 taper ratio. Thin interply resin layers are included in the model between the last set of dropped plies and the belt and core plies. Other configurations include different ply drop configurations; different thicknesses of the interply resin layers; and different stacking sequence of the belt, core, and dropped plies. The dimensions of the model, normalized by the ply thickness, are shown in Fig. 2 and the glass-epoxy and neat resin material properties assumed in the model are given in Table 1.

Location of Damage Onset

The location of damage onset in a tapered structure is assumed to coincide with the site of the *critical* stress state. Often this location is determined by first solving for the stress state via a given solution method and then using an appropriate damage onset criterion to determine the site of the critical stress state.

Finite-element analysis has been carried out for the baseline configuration with three different stacking sequences. In the first the belt plies form a $\{+45/-45\}_2$ sublaminate and the core plies form a $\{0\}_4$ sublaminate. In the second, the belt plies form a $\{0\}_4$ sublaminate and the core plies form a $\{+45/-45\}_2$ sublaminate. In both of these types, the three pairs of terminated plies are $\{+45/-45\}$ sublaminates. In the third stacking sequence, all of the plies are at 0° . These tapered stacking sequences are typically referred to by the stacking sequence of the thin sections: $[\pm 45_2/0_4]_S$, $[0_4/\pm 45_2]_S$, and $[0_8]_S$ respectively. Each ply and interply resin layer is modeled by a single layer of eight-node, 24-degree-of-freedom, solid brick elements based on the hybrid stress formulation. The resin regions that initiate at a ply drop are terminated with a six-node isoparametric pentahedral element. Initially, only one element is used in the width direction. A refined mesh of 84 elements that extends 20 elements to the left (decreasing x) of the last

ply drop, 40 elements to the right (increasing x), and 24 elements beginning at the junction of the interply resin layers. This refined mesh, shown in Fig. 3, has 80 elements that are $0.5t_{ply}$ long in the longitudinal direction and four elements that are $0.25t_{ply}$ long. The aspect ratios of the elements far away from the fine mesh region are relatively large; however, because those elements are essentially under an in-plane stress state the effect of the large aspect ratios on the stress state in the tapered region is negligible.

Whether or not thin resin layers are included can significantly alter the results. To investigate the effect of the resin layer thickness on the stress state, three different ratios of resin layer thickness to nominal ply thickness are assumed in the model: 0.10, 0.03, and 0.01. The results for the three different stacking sequences are illustrated in Figs. 4 to 6 for resin layers that are $0.1t_{ply}$ thick for a uniaxial displacement equivalent to a 1-MPa tensile load. In all cases, the maxima of the interlaminar normal and shear stresses at the ply drop are always greater than the values at the root of the taper. The results are similar for the other interply resin layer thicknesses. As summarized in Table 2, the peak interlaminar normal stresses increase slightly when the thickness of the interply resin layer decreases; however, the interlaminar shear stresses increase appreciably as the thickness decreases.

The best evidence of the damage initiation site is from experimental observation. An indication of failure initiating at the ply drop as proposed by Fish and Lee [2] is the failure mode described by Murri, et al. [3] for a unidirectional tapered laminate. Finite-element models were developed to determine the strain-energy release rate for delamination(s) growing between the dropped plies and the belt and/or core plies. One of their models was developed to “analyze delaminations observed in the test specimens.” This model, shown in Fig. 7, indicates that the root is not the site of damage initiation and that the ply drop might be the site of damage initiation for the unidirectional configuration. The loading in this case was cyclic tension-tension.

Other evidence of initiation was obtained in a series of tests designed to increase the structural integrity of tapered elements via structural tailoring [10]. Typically, the initial damage is catastrophic in nature. That is, under stroke control, delamination occurs as a *pop-in* phenomenon. Even if the test is stopped after the detection of damage, the failure surface often extends between the ply drop and the taper root, making the onset location indistinguishable. However, the overlapped-dispersed configuration studied in Ref. 10 had the characteristic of slow delamination growth. While under stroke control, a delamination was seen to occur at the location of the ply drop. The delamination grew across the width and extended slightly towards the taper root and then towards the thick section. This behavior was observed a number of times.

Other researchers have concluded that the taper root is the site of damage onset under static loads. For example in Ref. 3, the interlaminar normal stress was determined to be maximum at the taper root, the interlaminar shear at the taper root was determined to be on the same order as the interlaminar normal stress, and the interlaminar tensile strength was assumed to be less than the interlaminar shear strength. Thus, the stress state at the root was deemed to be critical,

even though at the ply drop the interlaminar shear stress was 3 times that at the root and the interlaminar normal stress was slightly lower than that at the root.

Although a categorical statement cannot be made, the evidence indicates that at least for some configurations the ply drop is the more critical site within a taper. In these cases, perhaps the taper root represents a geometric discontinuity as two plies diverge, and only limited load transfer is occurring. However, the ply drop may represent a more severe material discontinuity where load transfer is more significant.

Free-Edge and Taper Interaction

Wherever there is a discontinuity in a laminated composite structure, interlaminar stresses arise and can initiate delamination. In a finite-width tapered laminate, discontinuities occur at terminated plies and stress-free edges. Two-dimensional modeling of the tapered section cannot adequately include effects of stress-free edges.

The three-dimensional model with one element in the width direction cannot properly capture the effect of the stress-free edge. Accordingly, a model with seven elements in the width direction, a coarse three-dimensional representation, was used to elucidate the effect. The first four elements at the stress-free edge have transverse lengths of $1.0t_{ply}$. The next three elements have transverse lengths of 6, 30, and $60t_{ply}$, respectively. The finite-element model with one element in the width had 654 elements and 4350 degrees of freedom. The finite-element model with seven elements in the width had 4578 elements and 17,400 degrees of freedom. The three stacking sequences discussed earlier were analyzed with assumed resin layers of $0.1t_{ply}$. The results of particular note are given as surface and contour plots in Figs. 8 through 13 for the three interlaminar stresses in the bottom resin layer of the $[\pm 45_2/0_4]_S$ tapered laminate. In these figures only the region of interest—that is, $-10t_{ply}$ to $+10t_{ply}$ in the longitudinal direction about the ply drop, and from the stress-free edge to $4t_{ply}$ into the laminate—is displayed.

In these three figures, the three-dimensional effects are clear. The stress-free edge decreases the interlaminar normal stress σ_{zz} and increases the interlaminar shear stress σ_{zx} at the free edge. These effects may influence the prediction of free-edge delamination. A greater effect is seen in σ_{zy} .

When the interlaminar stress σ_{zy} is examined across the width at a location far away from a ply drop, the disturbance due to the stress-free edge is still substantial. The results from the models with one element and seven elements in the width are shown in Figs. 14 and 15 for σ_{zy} across the width in the bottom and top interply resin layers respectively. In a flat laminated plate, the edge effect is restrained to a boundary layer on the order of a few ply thicknesses. However, in these figures this boundary layer extends for more than $20t_{ply}$. Only in the center-most element of the seven-element model does the interlaminar shear stress approach zero. The

stress in the one-element model represents the average of two Gaussian points across the width and is inadequate in describing the profile of the interlaminar shear stress in the width direction.

The effect is greater at the ply drop. In Fig. 16, the interlaminar shear stress σ_{zy} in the bottom layer from the model with seven elements in the width is compared to the interlaminar shear stress from the model with one element in the width. The peak interlaminar shear stress occurs at $y = 3.5t_{ply}$ from the stress-free edge. Thus, the strip of elements in the longitudinal direction that contain the peak stress is displayed, rather than that at the edge. It is designated as “7-Element Edge” in the figure. Also presented in the figure are the values of the interlaminar shear towards the center of the three-dimensional model at $y = 70t_{ply}$. This curve is designated as “7-Element Near Center.” The effect of including additional elements in the width direction is considerable, increasing the peak interlaminar shear by more than a factor of 2. Different behavior is seen in the top resin layer in Fig. 17. Unlike the bottom layer which appears to be simply a constant decrement dependent on whether the location is before or after the ply drop, the interlaminar shear in the top layer is significantly different in shape between the one-element and seven-element models. Note that the model with one element in the width predicts a nonzero value for the interlaminar shear stress away from the ply drop, whereas the model with seven elements correctly shows the interlaminar stress at the center to be affected only near the ply drop. Although the full three-dimensional nature of the stress state at the stress-free edge and the ply drop is indicated by this coarse model, an accurate solution would require further refinement of the mesh at the stress-free edge.

Realistic Taper Geometries

Throughout most of the research performed on tapered sections, the geometry of the taper has been idealized as that shown in Fig. 1. This is sufficient if only a qualitative analysis is to be performed. Because variations due to manufacturing tolerances are common, the effect of process tolerances on nominal ply-drop geometries should be modeled for improved accuracy. The types of realistic ply-drop geometries previously considered in Ref. 11 are as-cured resin pockets, unsymmetric and offset ply-drop locations, varying ply thickness, and the occurrence of voids as illustrated in Fig. 18. These variations in the geometry occur as an artifact of the manufacturing process and cannot be avoided altogether even with proper handling. Specifically, the final shape of the resin pocket results as belt plies move into the air pocket at the termination of the ply. This air pocket is created when the immediate belt ply is placed on top of the dropped ply during the lay-up process. Misalignment of ply drops on the order of 1 to 2 mm occurs in hand-manufactured components. Typically, two halves of a symmetric tapered laminate are visually aligned and mated. Ply thickness variations are the natural response of the uncured composite to conform to the mold. Such thickness variations are the result of process permissible variations in cured ply thickness and the alignment of ply drops. Voids are the result of inadequate resin flow and the inability of removing the trapped air in the pocket.

In general, realistic ply-drop geometries can have a significant effect on the stress state when compared to models with ideal ply-drop geometries. Ill-formed pockets have the effect of increasing the local taper angle at the ply drop. Changing the local taper angle affects the stress state and can change the onset damage site. Misaligned or unsymmetric ply drops also greatly affect the interlaminar stress state and the von Mises stress. Again the predicted location of damage onset is dependent on the amount of offset of the ply drops. The interlaminar stresses are greatly increased in the presence of a void in the resin-rich pocket at the ply drop. In the finite-element analysis, the void can be approximated by reducing the stiffness of the resin elements at the ply drop by 6 orders of magnitude [11]. In general, analytical models that do not consider realistic taper geometries are inadequate in predicting the stress state.

Mode and Extent of Damage

The structural integrity is dependent on the damage growth in the taper region in addition to the initiation point. In most of the experimental evidence for tension-loaded, linear-tapered laminates, delamination is observed to initiate and grow unstably (i.e., pop in) under quasistatic load conditions [2,7–10]. Thus, delamination is deemed to be the initial failure mode and to be unstable in nature. However, the dispersed-overlapped configuration in Ref. 11 demonstrated stable growth under quasistatic loading. Damage initiated at the ply drop and occurred mostly above the ply drop, and no unstable delamination growth was observed.

The finite-element model can be used to examine the progressive failure of elements by applying a failure criterion to the matrix elements. The modulus of the element with the greatest von Mises stress is reduced by a factor of 10^6 to simulate failure. The stresses are then recalculated with the *failed* element. This process is repeated for a number of iterations. Note that this does not take into consideration the internal stress-free boundary nor the singularity that may result at the front of the propagating crack.

In Fig. 19, the displacement versus the number of elements failed is shown for the overlapped-dispersed configuration considered in Ref. 10. This displacement is normalized by the displacement of the tapered structure at damage initiation. As shown in the figure, after the initial failure, almost 30 elements will fail instantaneously if the stroke is not reduced at the onset of damage. After this a small increase in the stroke will result in a substantial instantaneous failure of elements. In Fig. 20, the failed elements are highlighted via bold lines. The order of failure is designated by the shading of the element and corresponds to the scale near the bottom of Fig. 19. The lightest element failed first; the darkest element failed last. The model predicts that delamination will initiate in the lower resin layer and progress for some time. At some point delamination will initiate in the upper layer. Both delamination fronts will grow towards the thick and thin sections of the tapered laminate. Unfortunately, these results of the numerical simulation do not agree with experimental observation.

If the two resin elements immediately adjacent to the dropped plies are assumed to be failed, the progressive damage model predicts a change in the growth characteristics and failure surface. Fig. 21 shows that the delamination grows in a stable fashion after 40 elements have failed when an initial flaw in the resin pocket is assumed. Unlike the unflawed case, greater and greater displacements are needed to cause growth of the delamination. This concurs with the experimental observation. The model predicts two delamination fronts that both grow towards the thick section as shown in Fig. 22. Delamination initiates in the upper interply resin layer and always remains ahead of the delamination in the lower interply resin layer. This coincides with the experimental observation.

When the resin pocket is intact, the progressive damage model does not predict the stable growth that is observed in experiments. When the elements at the ply drop are initially failed, the model does predict stable growth. To validate the model further, a ply-drop configuration that exhibited unstable growth is modeled with a failed resin pocket. The staircased-dispersed configuration is also contained in Ref. 11 and exhibited a pop-in failure of delamination. The progressive damage model predicts this unstable growth as shown in Fig. 23. Even after 50 elements have failed, the normalized displacement to cause additional damage is approximately 15% less than the displacement necessary to initiate damage. The model predicts two delamination fronts that grow from the failed region of the resin pocket. The surface is different than the dispersed-overlapped configuration in that the damage initiates in the upper interply resin layer but is eventually dominated by the delamination in the lower layer as shown in Fig. 24. In this configuration the damage grows towards both the thick and thin sections of the tapered element as was observed experimentally. Thus, the progressive damage model correctly predicts stable and unstable growth only if initial damage is assumed.

Physical Representation

Often, the belt plies are assumed to be aligning themselves with respect to the longitudinal axis under uniaxial tension [6]. This is used to explain why the interlaminar normal stress goes from a compressive value just prior to the ply drop to a tensile value just after the ply drop. This is a simplistic idealization of the taper section, and it appears to be inadequate.

Consider the spring model in Fig. 25, where the resin-rich pockets are simplified as an elastic foundation of varying thickness and the belt and core plies as rigid elements. An interply resin layer is included in this model as a constant-thickness layer in the elastic foundation. Translation in the local z direction (\hat{z}) results in tensile stresses in the foundation for a positive w or compressive stresses for a negative w . These stresses are inversely proportional to the local foundation thickness and are given by:

$$\sigma_{zz} = E_f \frac{w}{t_f} \quad (1)$$

where E_f is the elastic modulus of the foundation and t_f is the local foundation thickness. A singularity develops at the ply drop if a zero-thickness interply resin layer is assumed (i.e., no interply resin layer). Rotation of the belt plies results in tensile and compressive stresses proportional to the distance from the center of rotation and inversely proportional to the local foundation thickness. For small angles the stress is approximately

$$\sigma_{zz} = E_f \frac{\tilde{x}\alpha}{t_f} \quad (2)$$

where \tilde{x} is the longitudinal coordinate in the local axes. Stress distributions for translation and rotation of the rigid belt plies are shown in Fig. 26. Also included at the top of the figure is a graphical representation of the foundation thickness. The stresses are normalized by the deflection (w or α), the elastic modulus of the foundation, and the assumed thickness of the resin layer, t_r . Any realignment of the belt plies results in a stress state that is a linear combination of the stresses due to w and α . Although the compressive stress prior to the ply drop might be approximated by a $-w$ displacement, the peak tensile stress after the ply drop cannot be approximated by any combination of w and α .

Conclusions

The structural integrity of tapered composite beams has been investigated. Finite-element modeling and experimental observations allow for greater insights in the controlling failure mechanisms. In particular the following conclusions are made:

1. Damage initiates at the ply drop and not at the root of the taper for the configurations studied.
2. The effects of the taper and the stress-free-edge discontinuities cannot be decoupled. Three-dimensional modeling of the tapered region is needed for adequate inclusion of the stress-free-edge effects.
3. Common artifacts of the manufacture and cure processes tend to increase the local effective taper angle, thus increasing the interlaminar stress state and decreasing the structural integrity. Of particular note are voids or cracks in the resin pocket.
4. The progressive failure model indicates that the resin pocket is failed prior to onset of delamination. The model is capable of predicting both stable and unstable delamination growth.
5. The interlaminar stress state cannot be adequately explained by the alignment of the belt plies.

Acknowledgments

The authors wish to thank their former students, Anthony D. Botting, John C. Fish, and Antonio S. Llanos, who have contributed to the research on tapered structures. This work was supported by the Army Research Office under Contract DAAL-03-88-C002. Thomas Doligalski was the contract monitor.

References

1. Chan, W. S. and Phillips, N. B., "Structurally Efficient Composite Main Rotor Hub Flexures," USAAVSCOM TM-87-D-4, Dec. 1988.
2. Fish, J. C. and Lee, S. W., "Delamination in Tapered Composite Structures," *Engineering Fracture Mechanics*, Vol. 34, (1), 1989, pp. 43-54.
3. Murri, G. B., Salpekar, S. A., and O'Brien, T. K., "Fatigue Delamination Onset Prediction in Unidirectional Laminates," Composite Materials: Fatigue and Fracture, ASTM STP 1110, American Society for Testing and Materials, Philadelphia, 1991, pp. 312-339.
4. Murri, G. B., O'Brien, T. K., and Salpekar, S. A., "Tension Fatigue of Glass/Epoxy and Graphite/Epoxy Tapered Laminates," *American Helicopter Society Journal*, Vol. 38, (1), Jan. 1993, pp. 29-37.
5. Salpekar, S. A., Raju, T. S., and O'Brien, T. K., "Strain Energy Release Rate Analysis of Delamination in a Tapered Laminate Subjected to Tension Load," *Proceedings of the American Society for Composites Third Technical Conference*, Seattle, WA, September 1988, pp. 642-654.
6. Aramanios, E. A. and Parnas, L., "Delamination Analysis of Tapered Laminated Composites Under Tensile Loading," *Composite Materials: Fatigue and Fracture, ASTM STP 1110*, American Society for Testing and Materials, Philadelphia, 1991, pp. 340-358.
7. Llanos, A. S. and Vizzini, A. J., "The Effect of Film Adhesive on the Delamination Strength of Tapered Composites," *Journal of Composite Materials*, Vol. 26, No. 13, 1992, pp. 1968-1983.
8. Botting, A. D., Vizzini, A. J., and Lee, S. W., "The Effect of Ply-Drop Configuration on the Delamination Strength of Tapered Composite Structures," *Proceedings of the AIAA/ASME/ASCE/AHS/ASC 33rd Structures, Structural Dynamics, and Materials Conference*, Dallas, Texas, April 1992, pp. 40-47.

9. Fish, J. C. and Vizzini, A. J., "Tailoring Concepts for Improved Structural Performance of Rotorcraft Flexbeams," *Composites Engineering*, Vol. 2, (5-7), 1992, pp. 303-312.
10. Fish, J. C. and Vizzini, A. J., "Delamination of Ply-Drop Configurations," Composite Materials: Testing and Design, 11th Symposium, ASTM STP 1206, American Society for Testing and Materials, Philadelphia, PA, pp. 323-332.
11. Vizzini, A. J., "Influence of Realistic Ply-Drop Geometries on Interlaminar Stresses in Tapered Laminates," *Composite Materials: Fatigue and Fracture*, American Society for Testing and Materials, Philadelphia, in press.

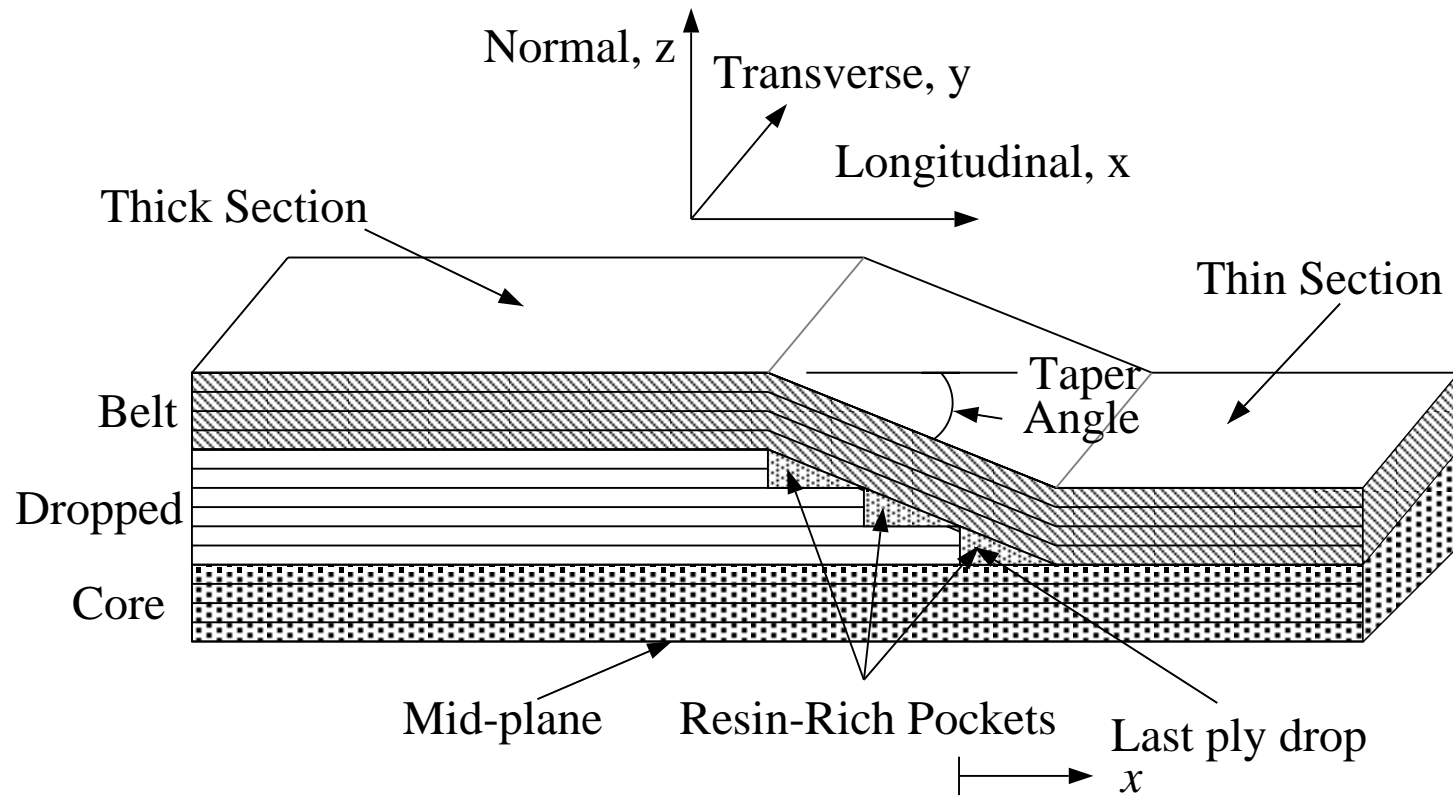


Figure 1 Schematic diagram of tapered specimen

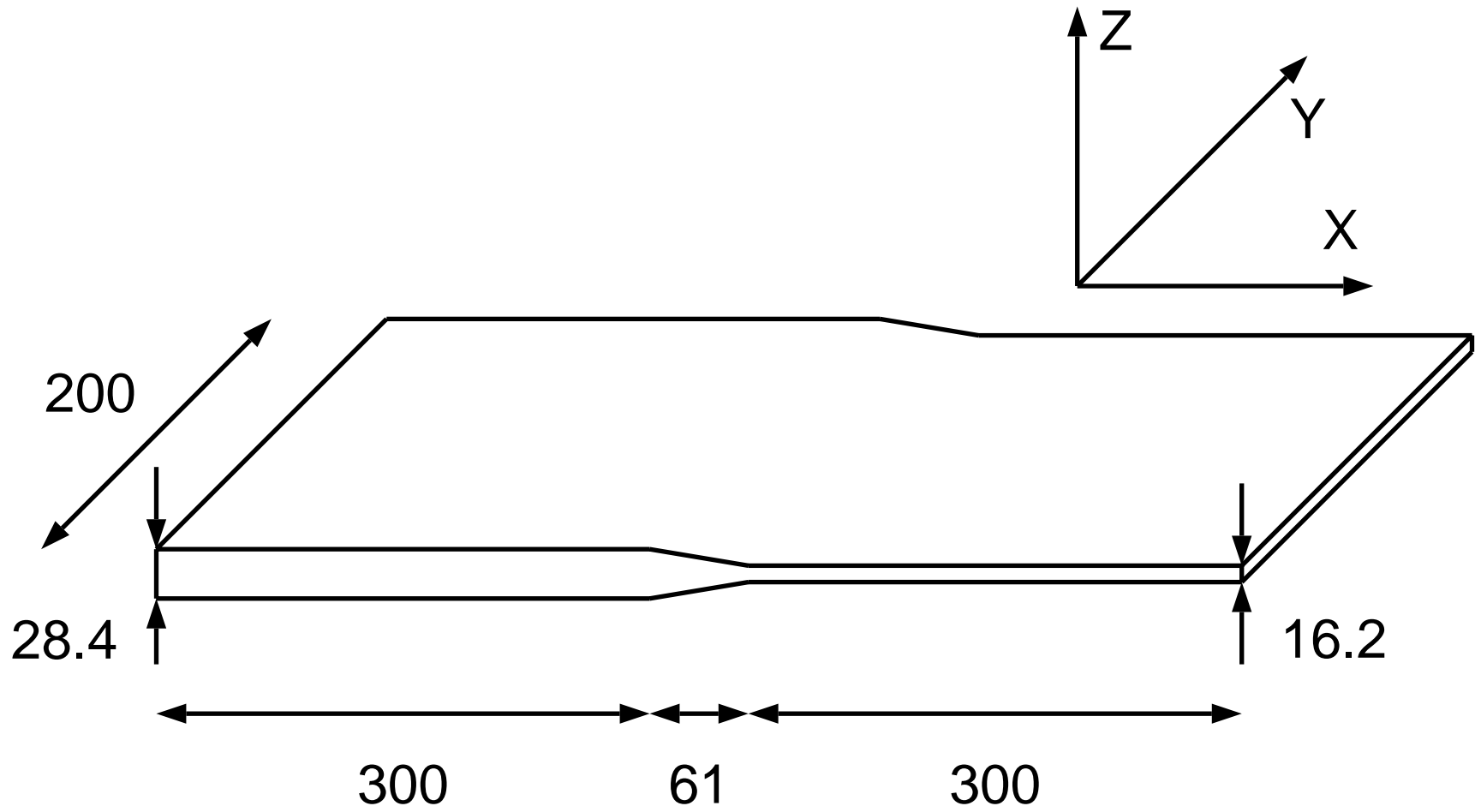


Figure 2 Dimensions of baseline specimen normalized by ply thickness

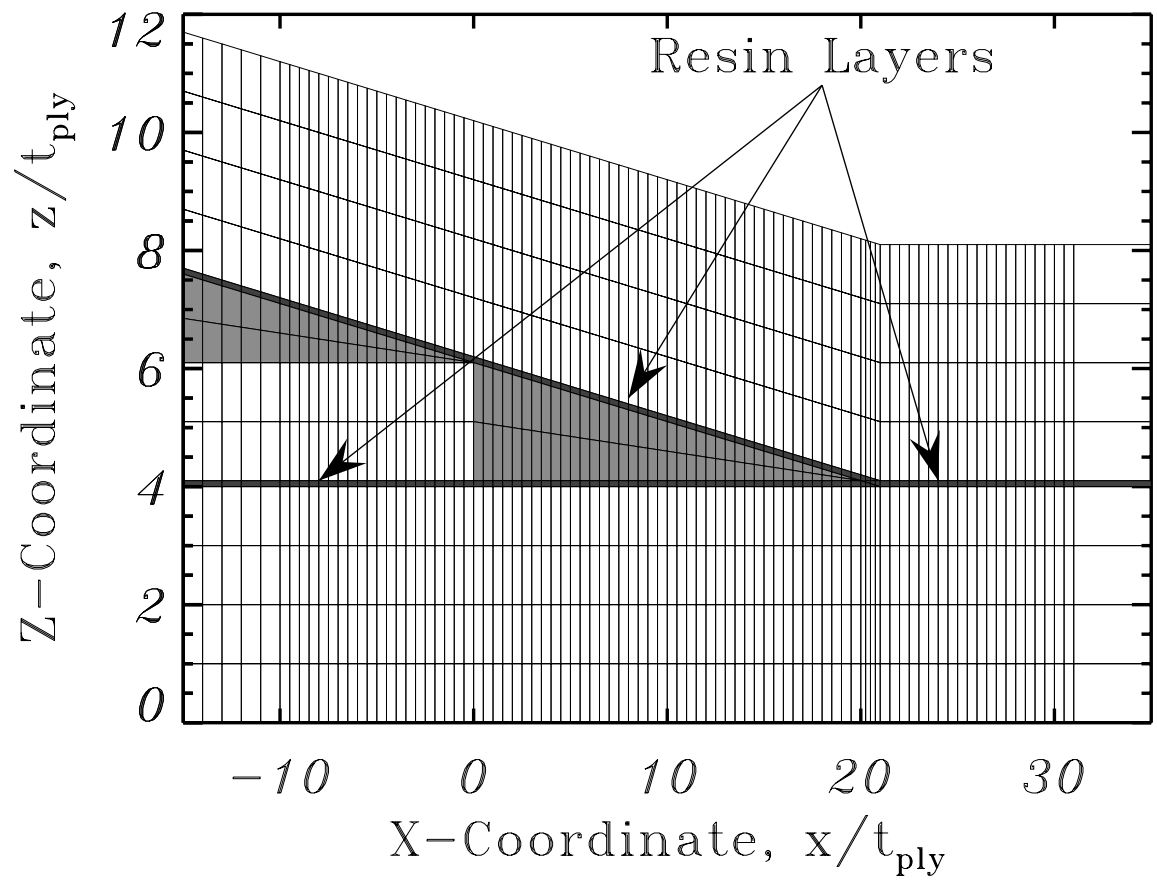


Figure 3 Finite element mesh for determination of critical location

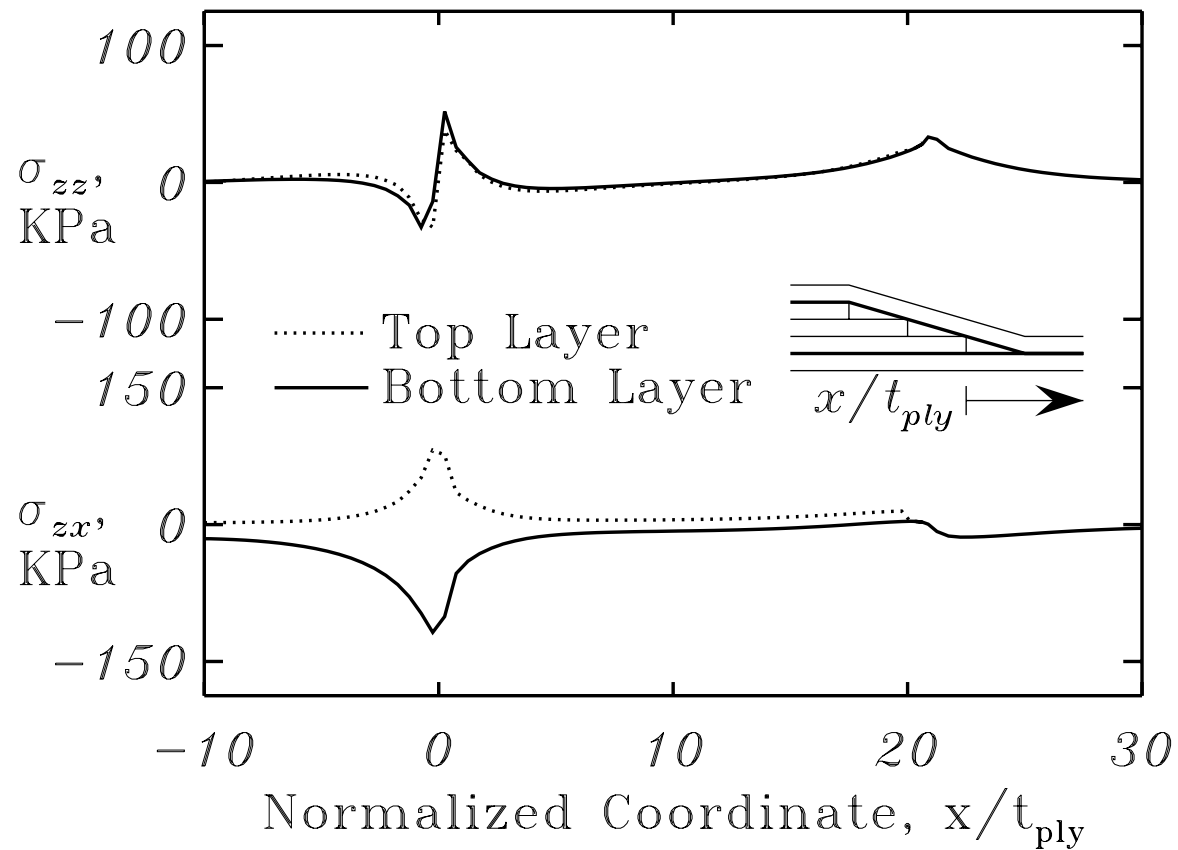


Figure 4 Interlaminar stresses for $[\pm 45_2/0_4]_s$ with resin layers of $0.1t_{ply}$

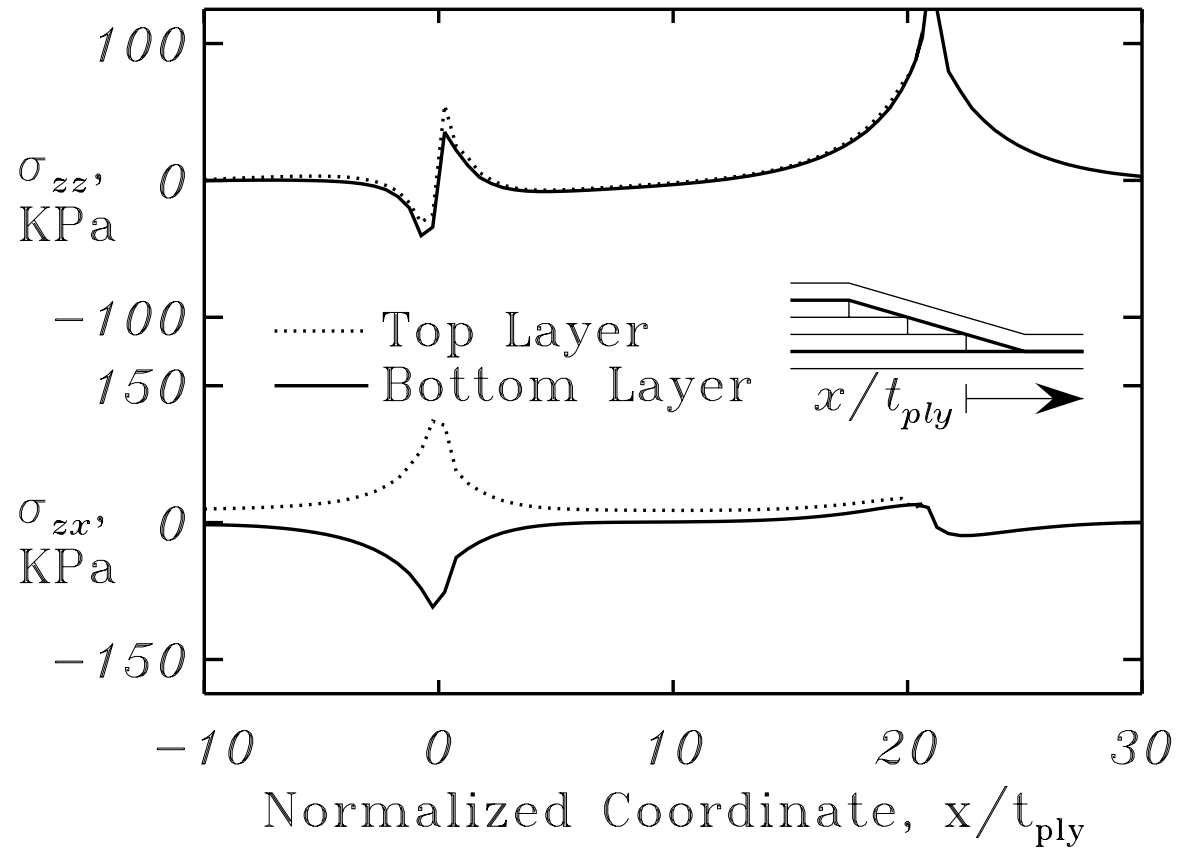


Figure 5 Interlaminar stresses for $[0_4/\pm 45_2]_s$ with resin layers of $0.1t_{ply}$

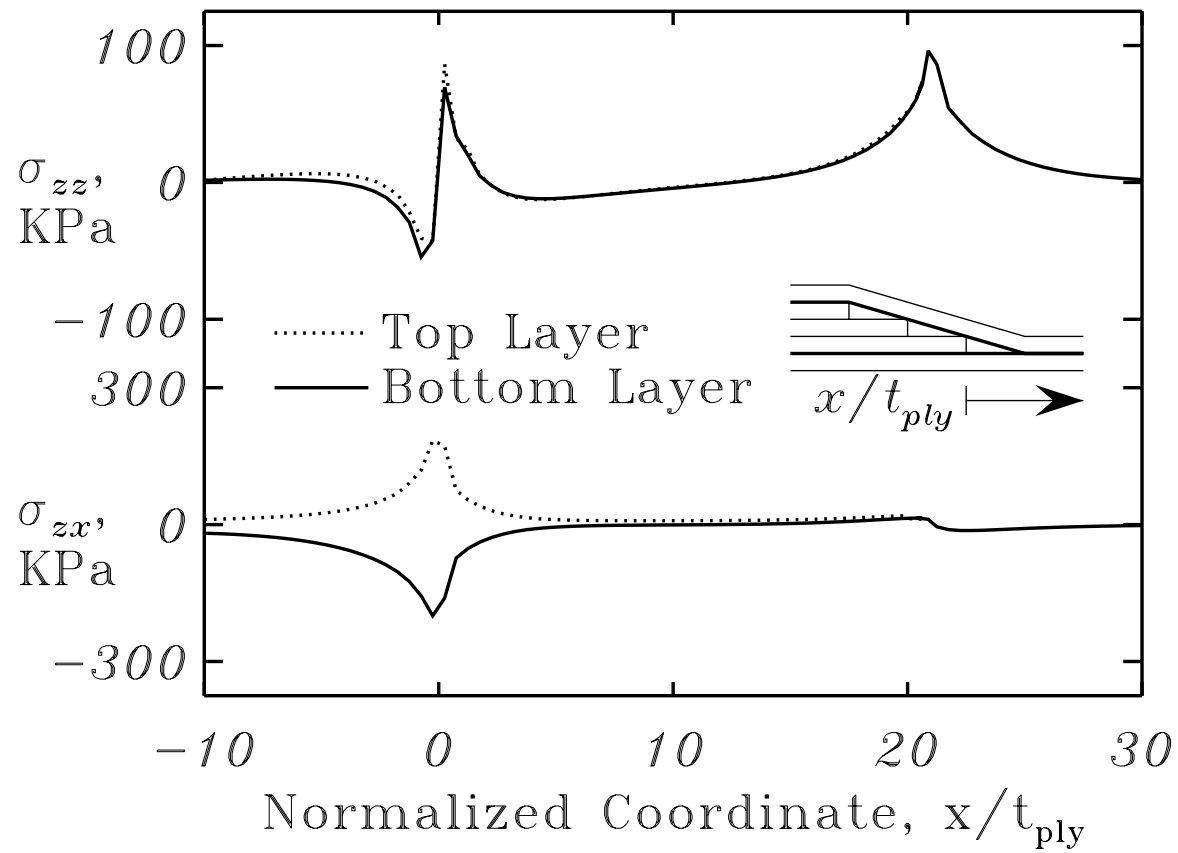


Figure 6 Interlaminar stresses for $[0_8]_s$ with resin layers of $0.1t_{ply}$

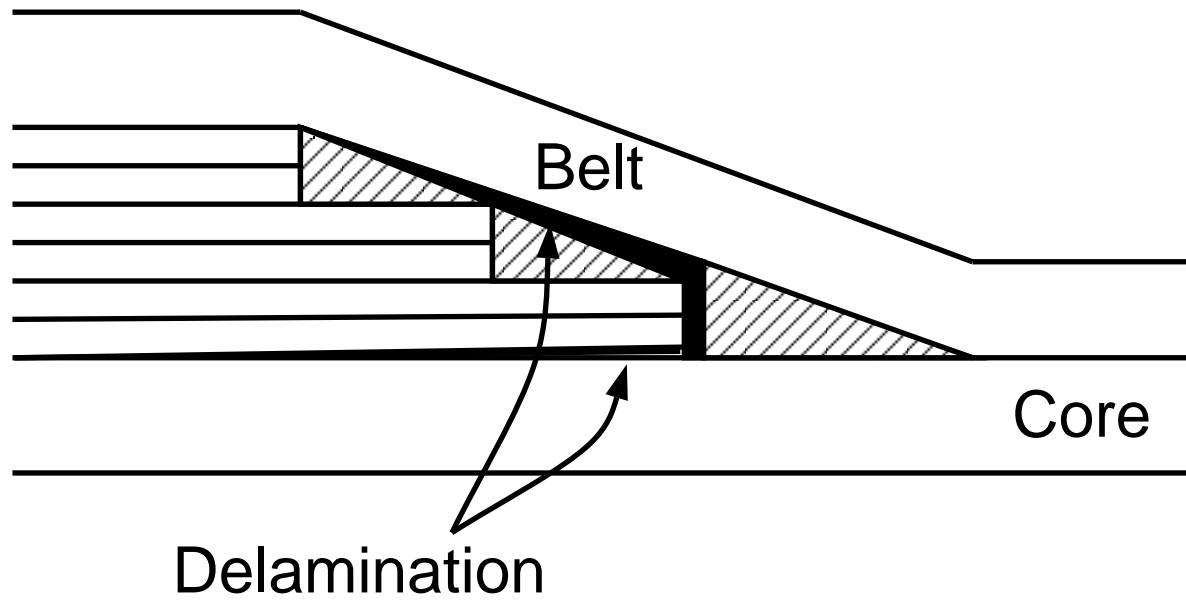


Figure 7 Schematic diagram of initial delamination damage [3]

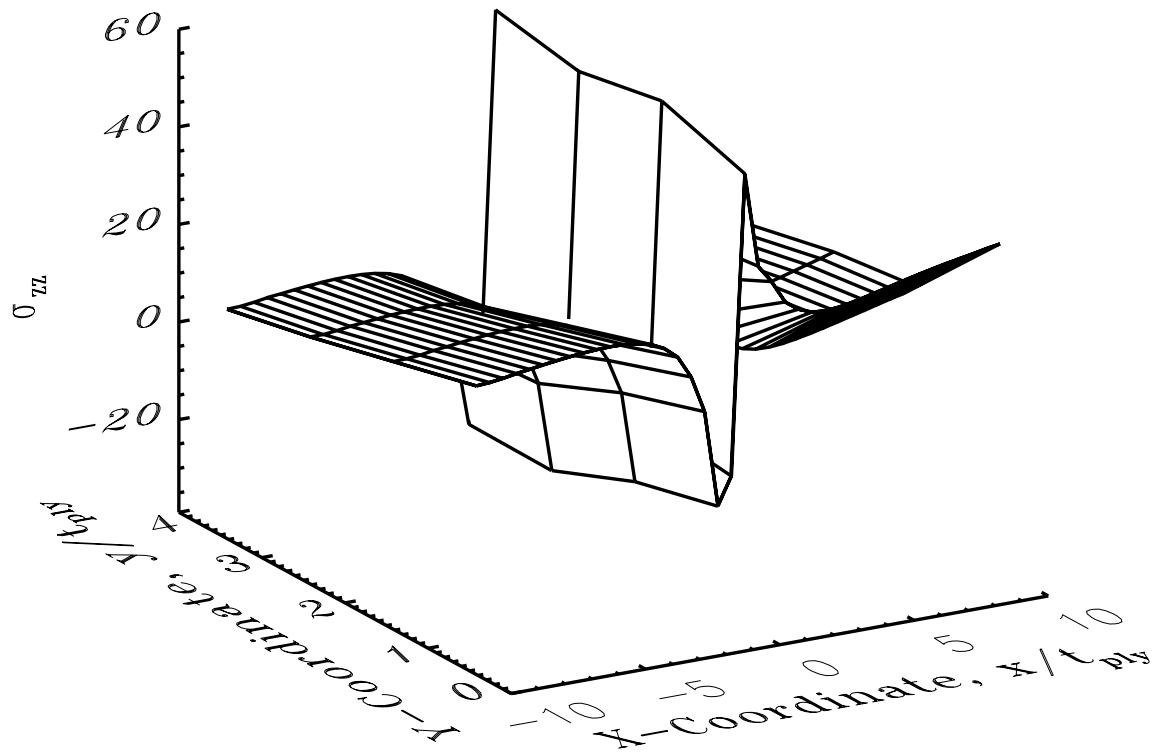


Figure 8 Surface plot of interlaminar normal stress σ_{zz} for $[\pm 45_2/0_4]_S$ in the bottom resin layer

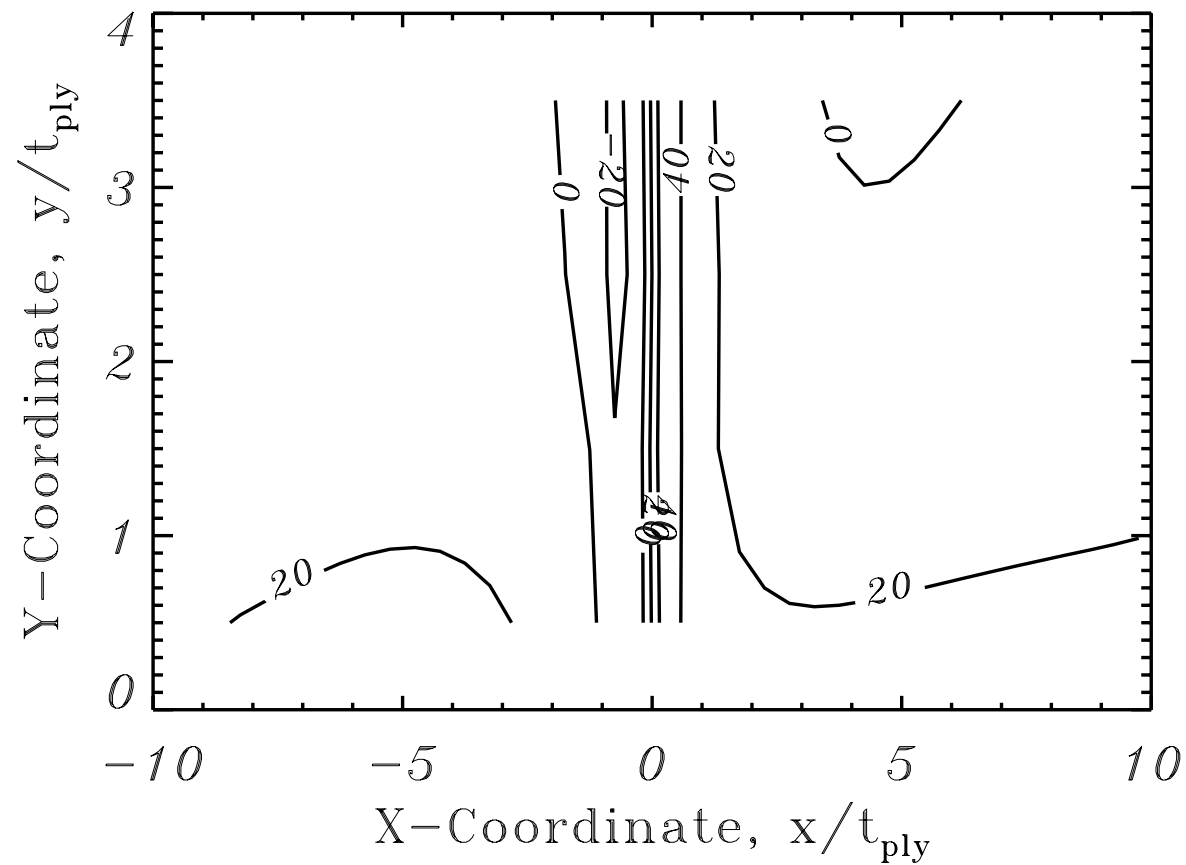


Figure 9 Contour plot of interlaminar normal stress σ_{zz} for $[\pm 45_2/0_4]_S$ in the bottom resin layer

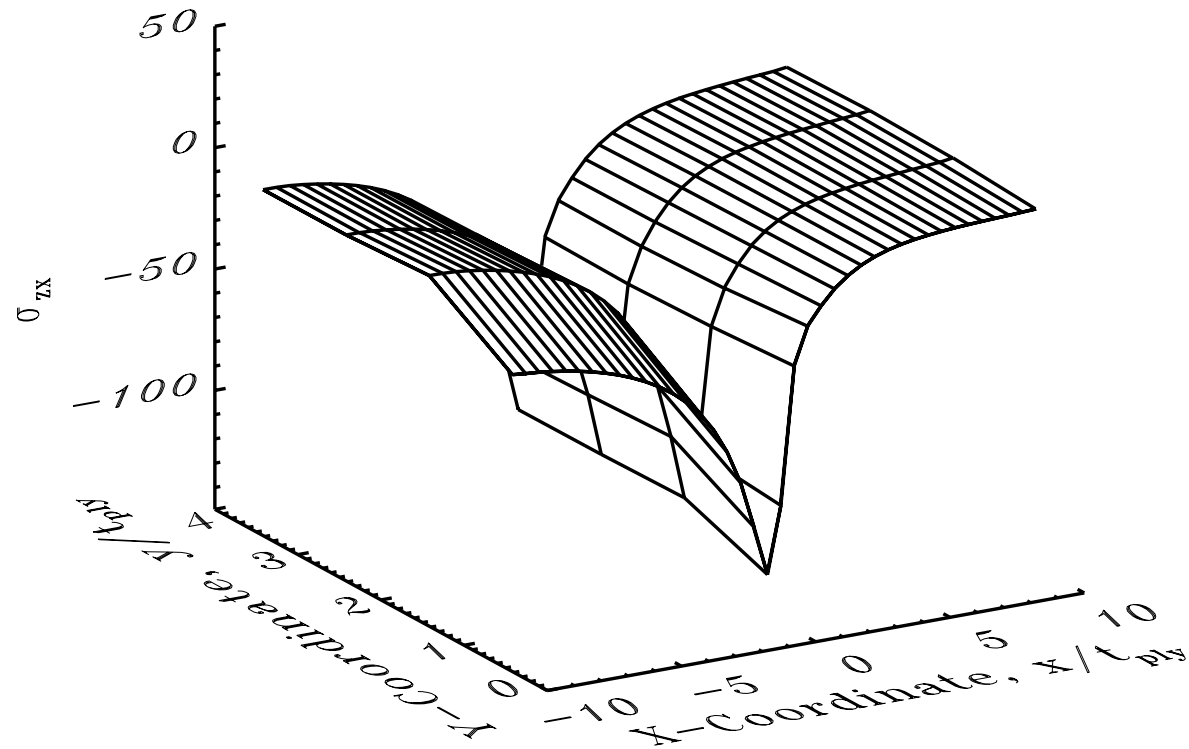


Figure 10 Surface plot of interlaminar shear stress σ_{zx} for $[\pm 45_2/0_4]_S$ in the bottom resin layer

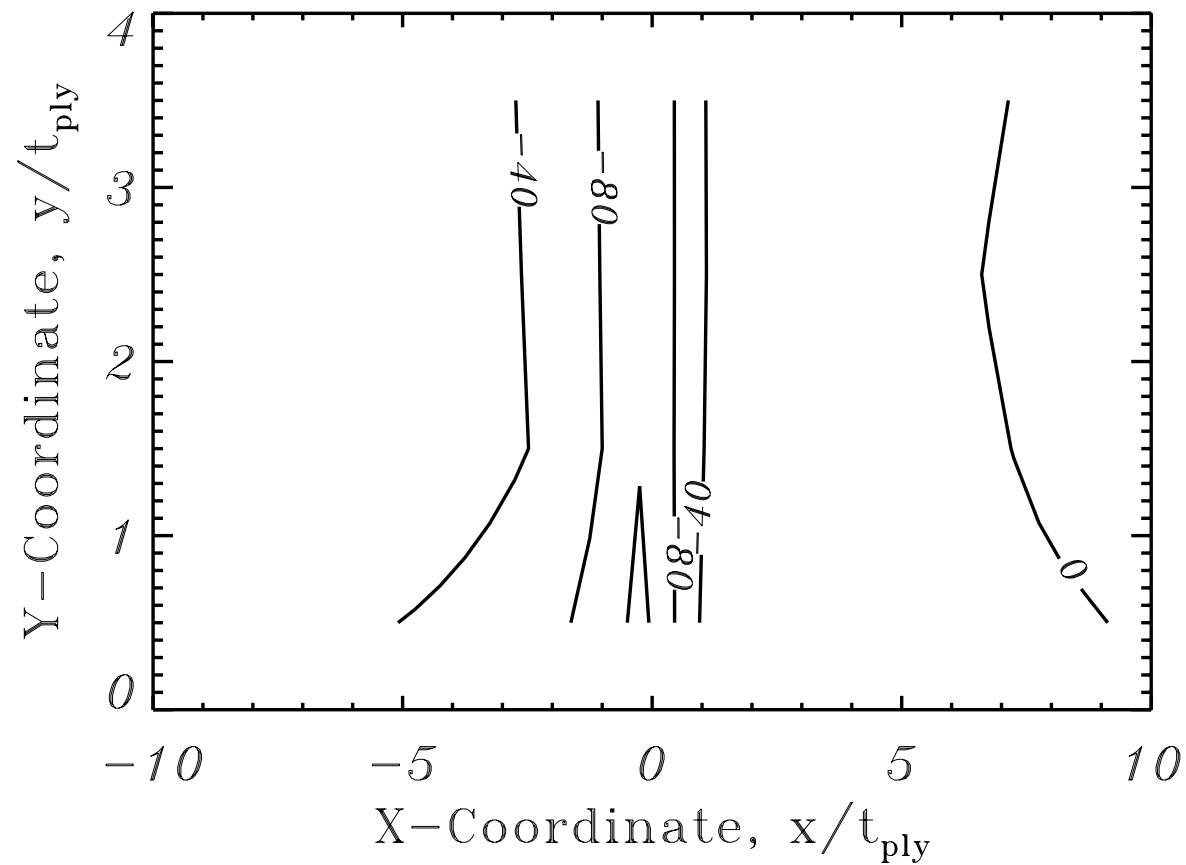


Figure 11 Contour plot of interlaminar shear stress σ_{zx} for $[\pm 45_2/0_4]_S$ in the bottom resin layer

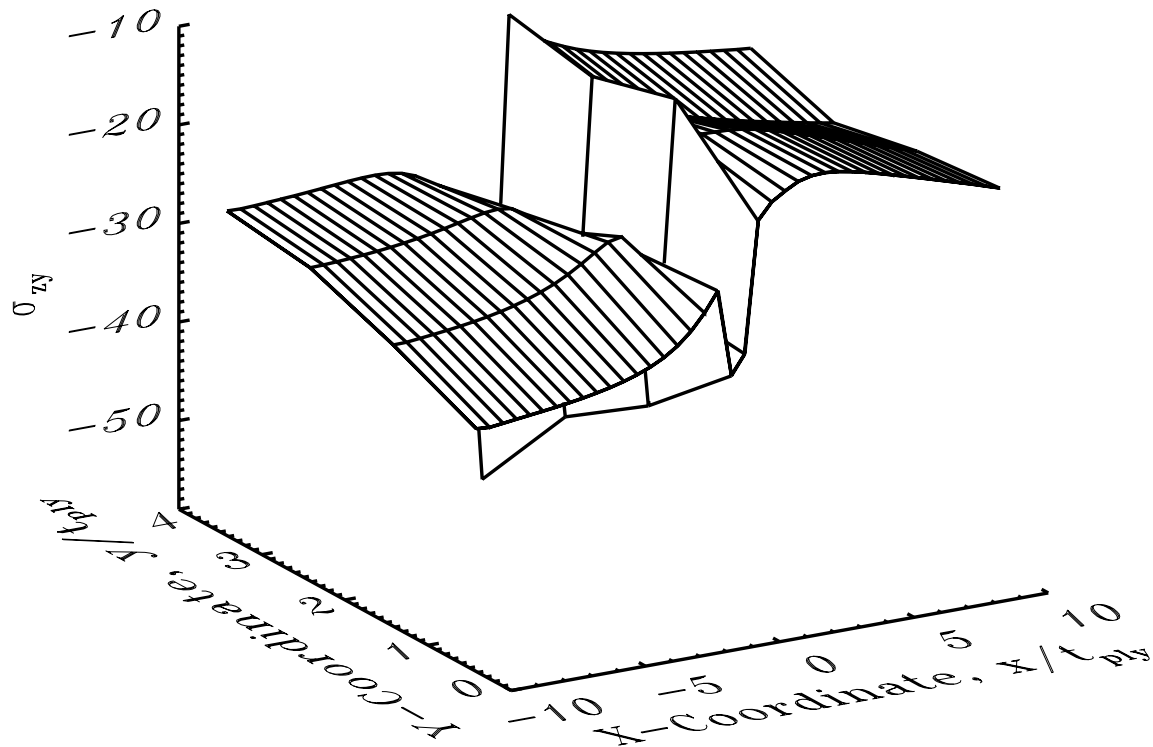


Figure 12 Surface plot of interlaminar shear stress σ_{zy} for $[\pm 45_2/0_4]_S$ in the bottom resin layer

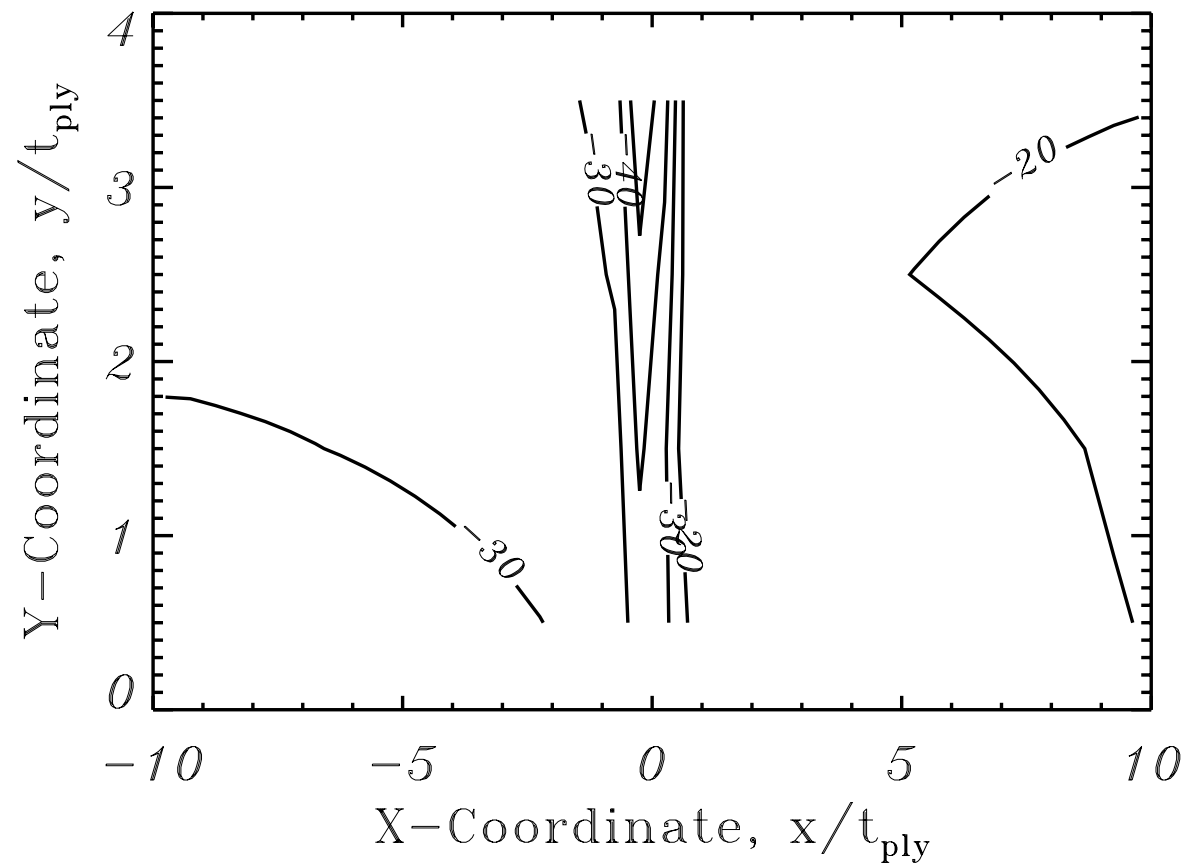


Figure 13 Contour plot of interlaminar shear stress σ_{zy} for $[\pm 45_2/0_4]_S$ in the bottom resin layer

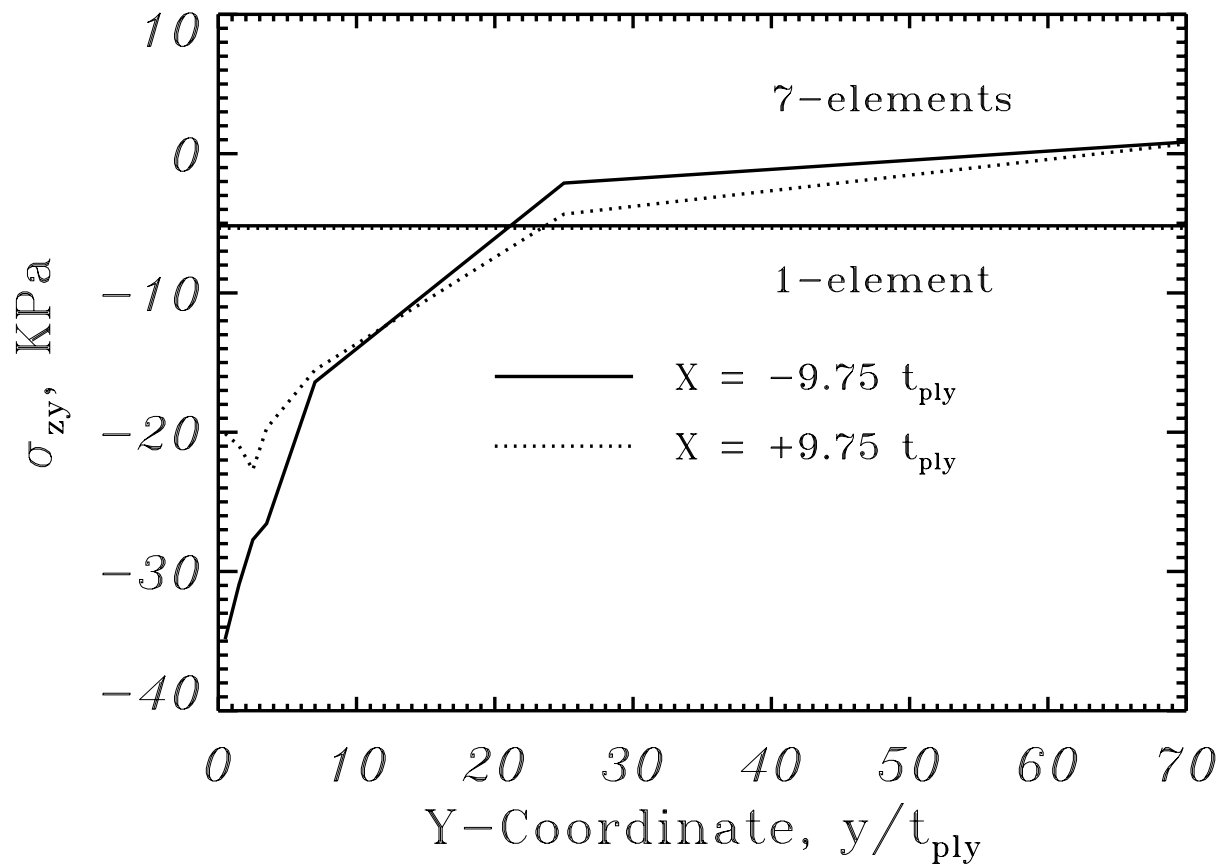


Figure 14 Comparison of interlaminar shear stress σ_{zy} for $[\pm 45_2/0_4]_S$ in the bottom resin layer

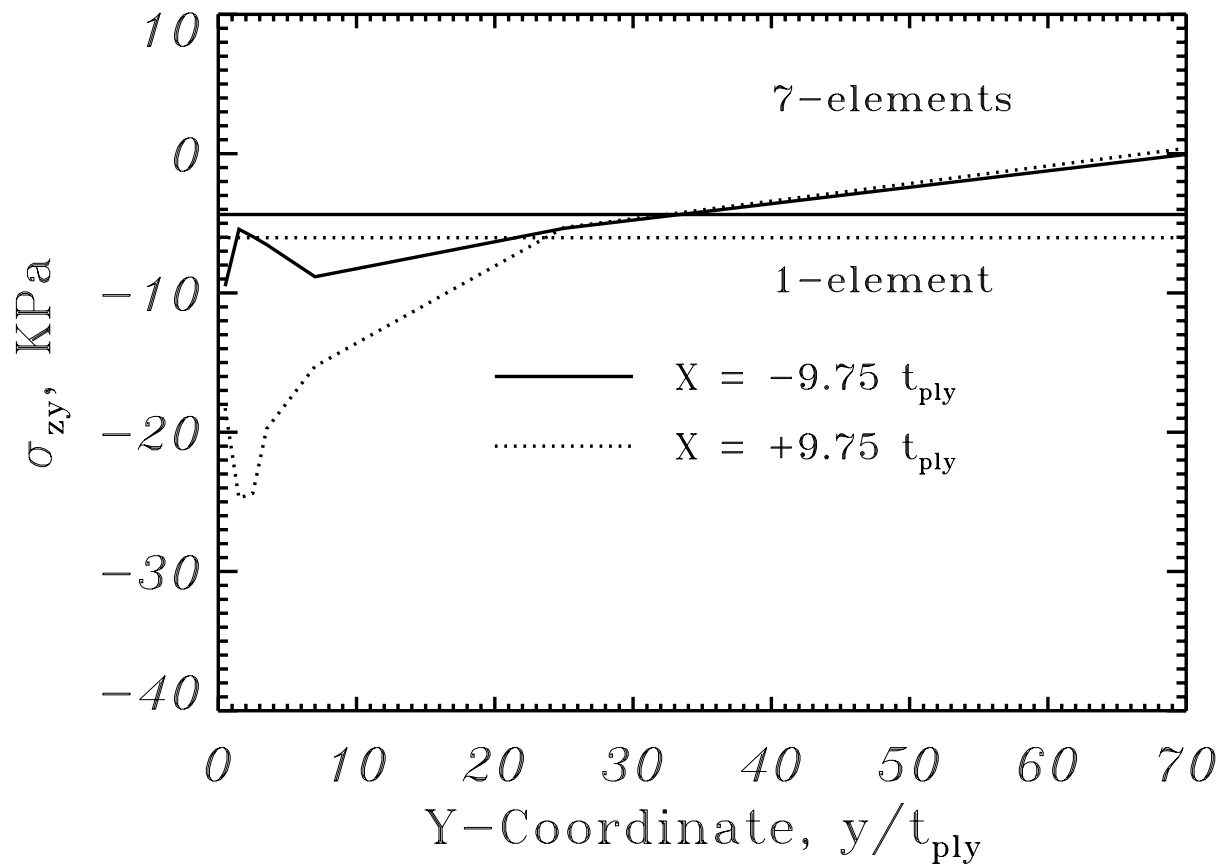


Figure 15 Comparison of interlaminar shear stress σ_{zy} for $[\pm 45_2/0_4]_S$ in the top resin layer

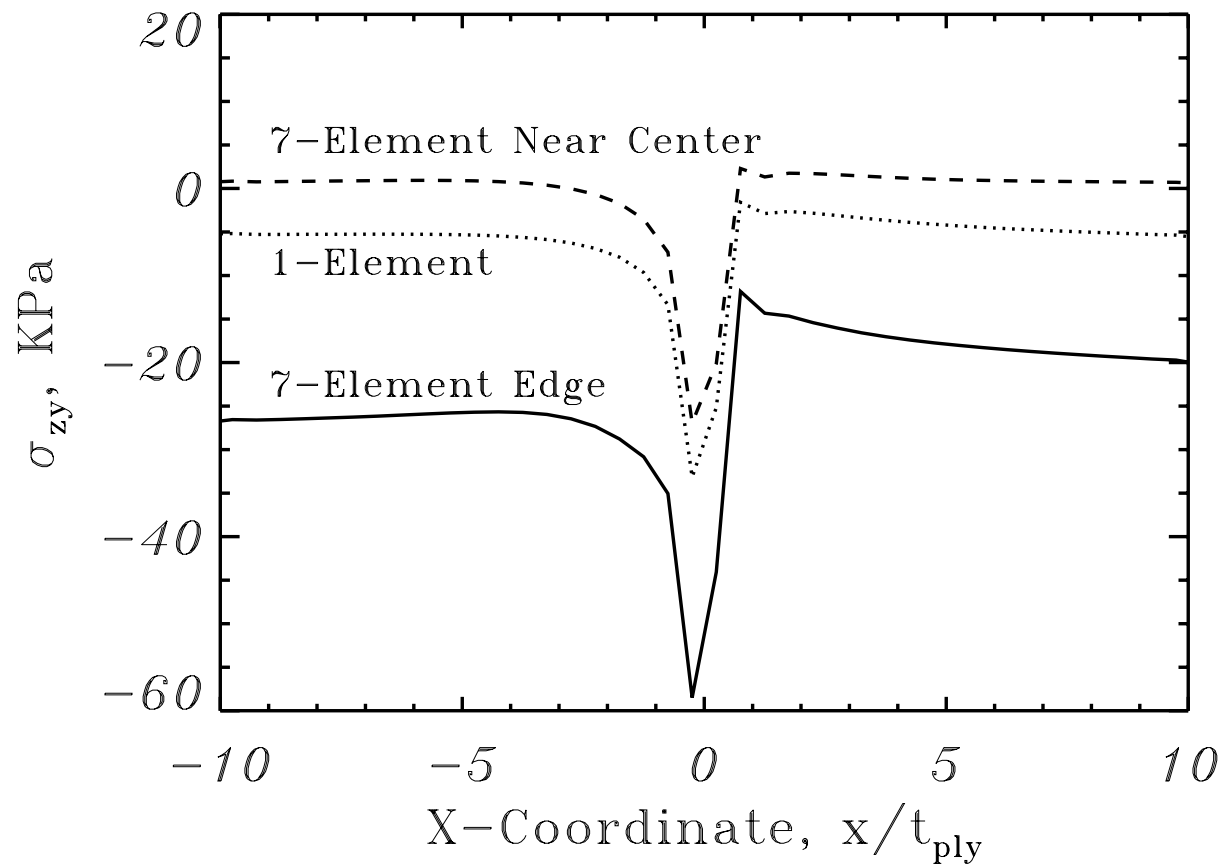


Figure 16 Comparison of interlaminar shear stress σ_{zy} for $[\pm 45_2/0_4]_S$ in the bottom resin layer

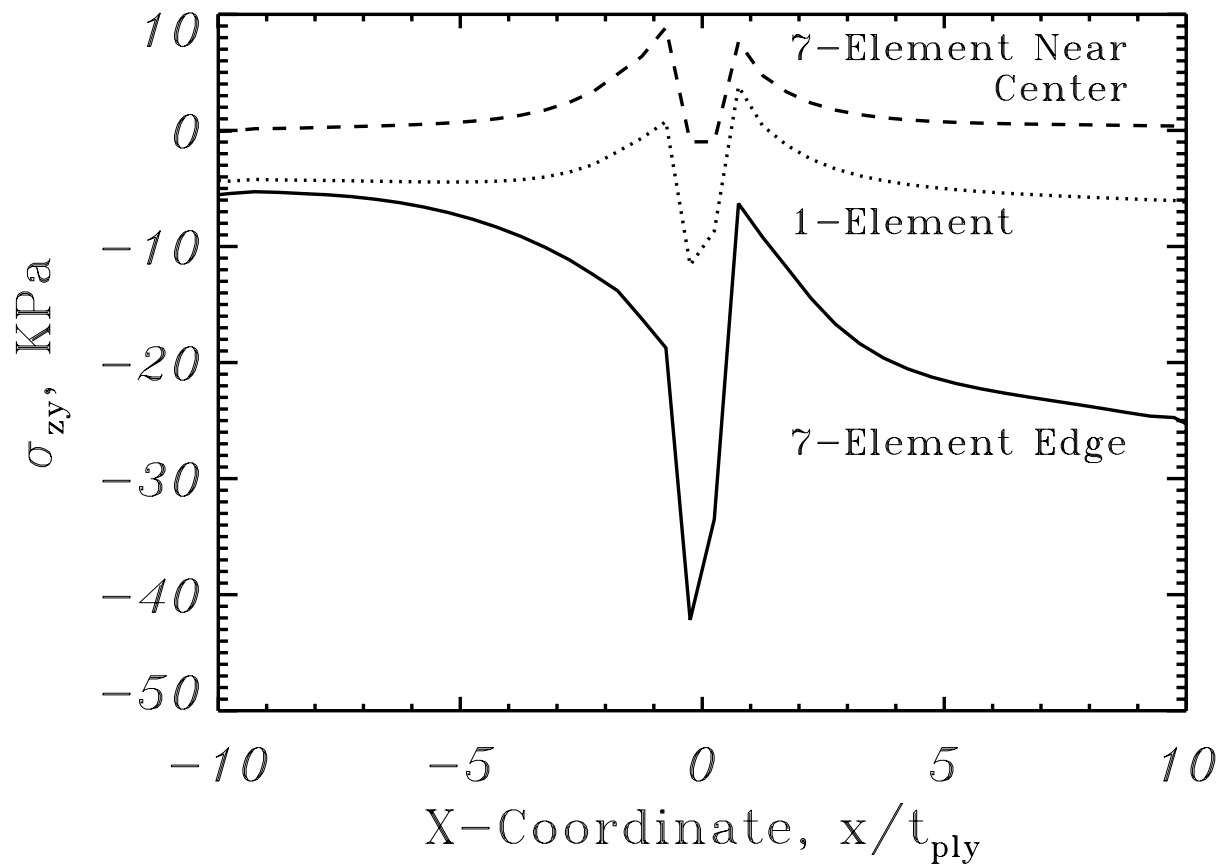


Figure 17 Comparison of interlaminar shear stress σ_{zy} for $[\pm 45_2/0_4]_S$ in the top resin layer

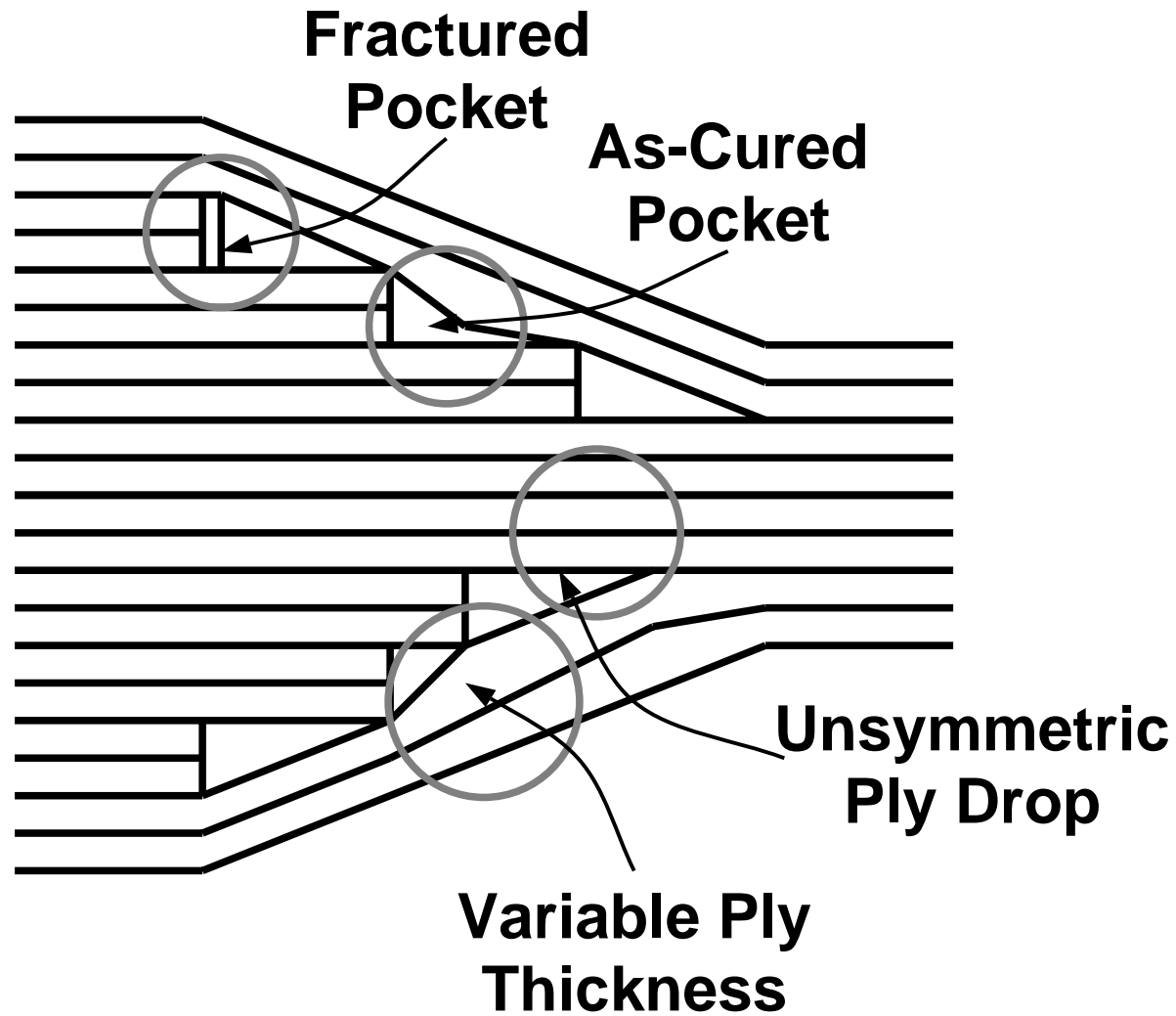


Figure 18 Schematic drawing of realistic taper geometries

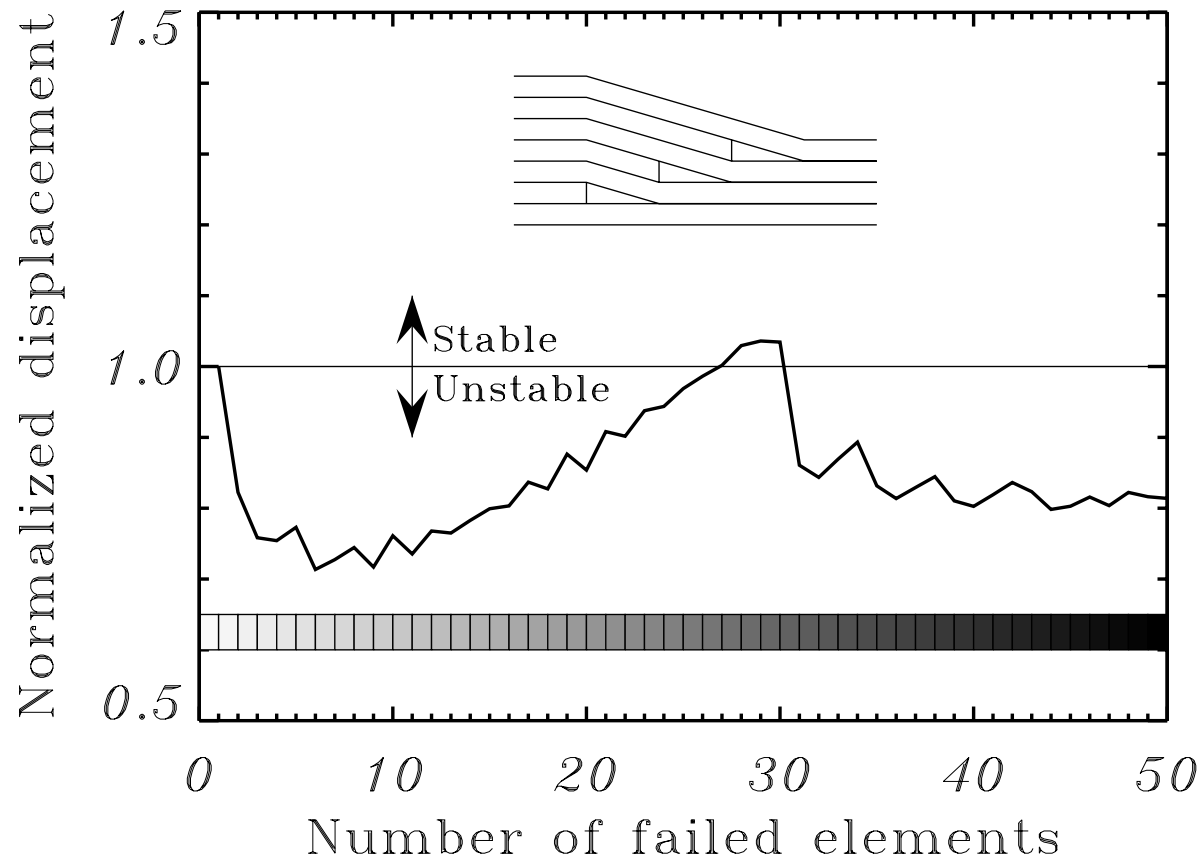


Figure 19 Normalized axial displacement versus number of failed elements for unflawed overlapped-dispersed configuration

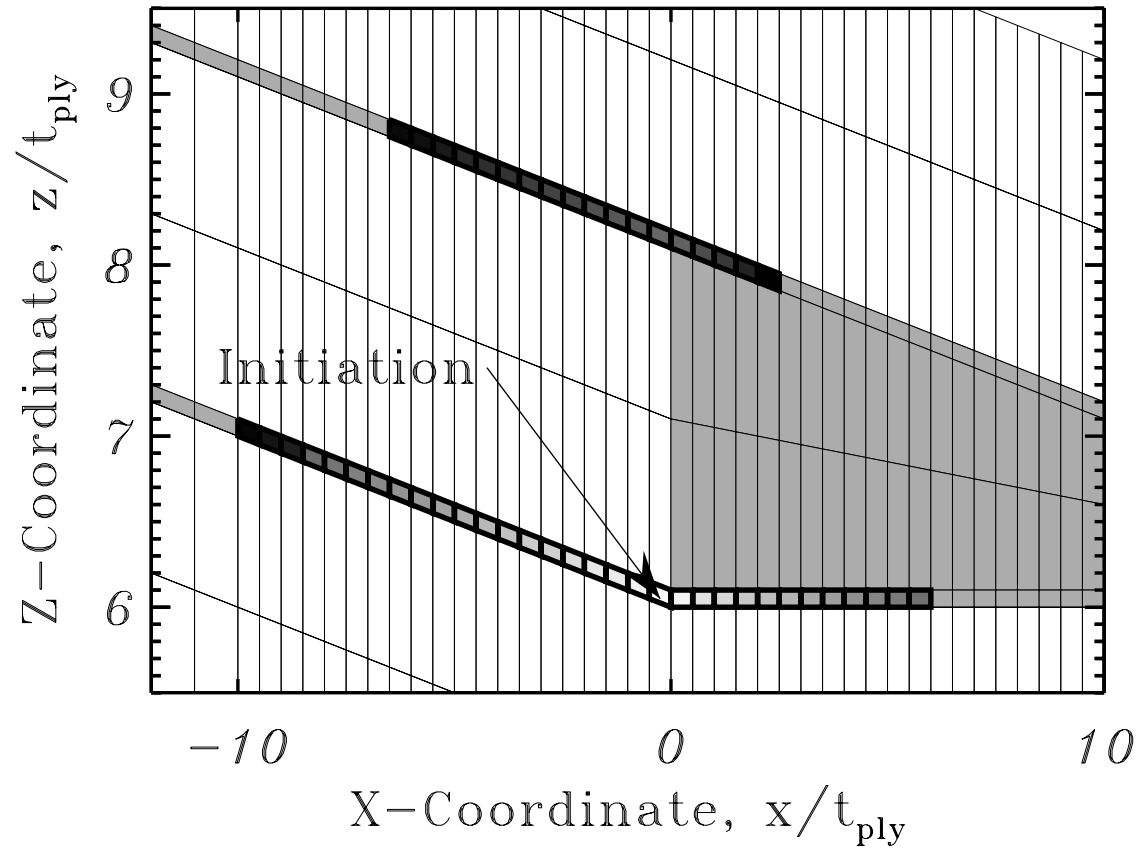


Figure 20 Delamination propagation for unflawed overlapped-dispersed configuration

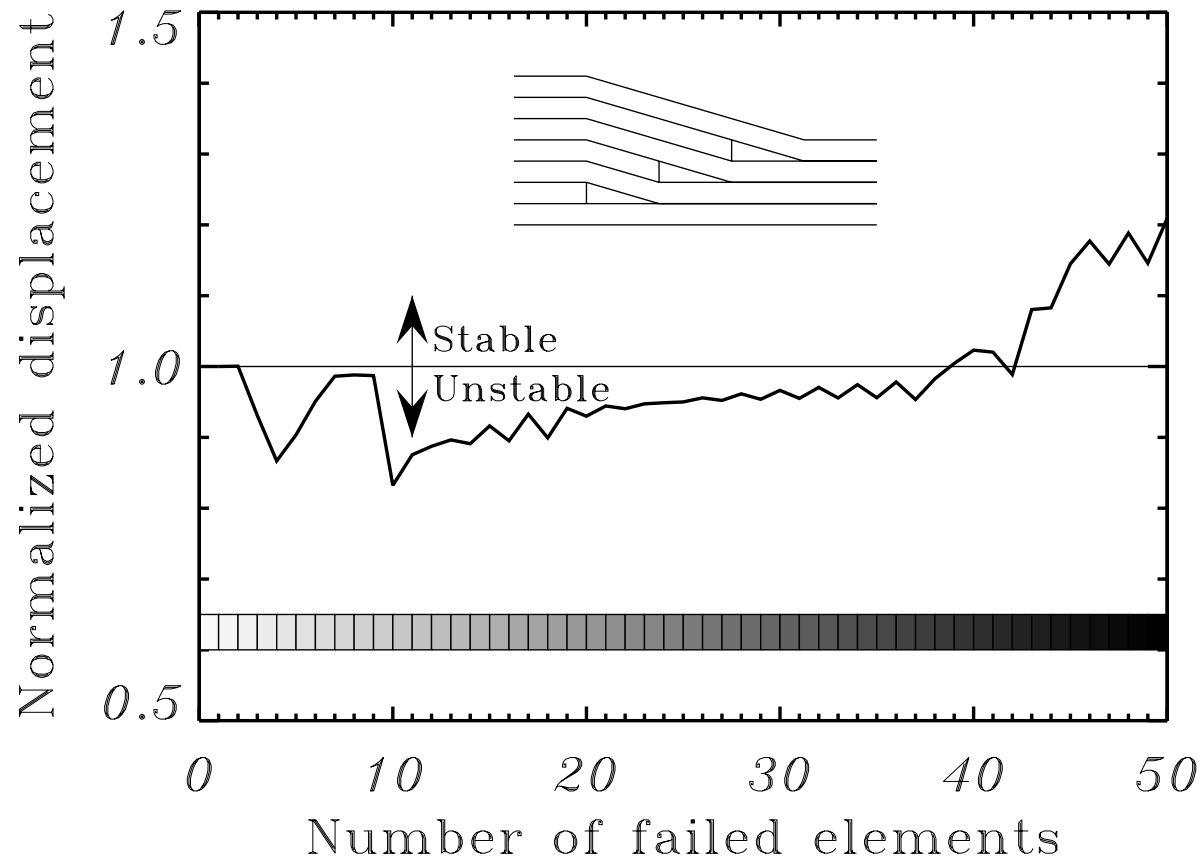


Figure 21 Normalized axial displacement versus number of failed elements for flawed overlapped-dispersed configuration

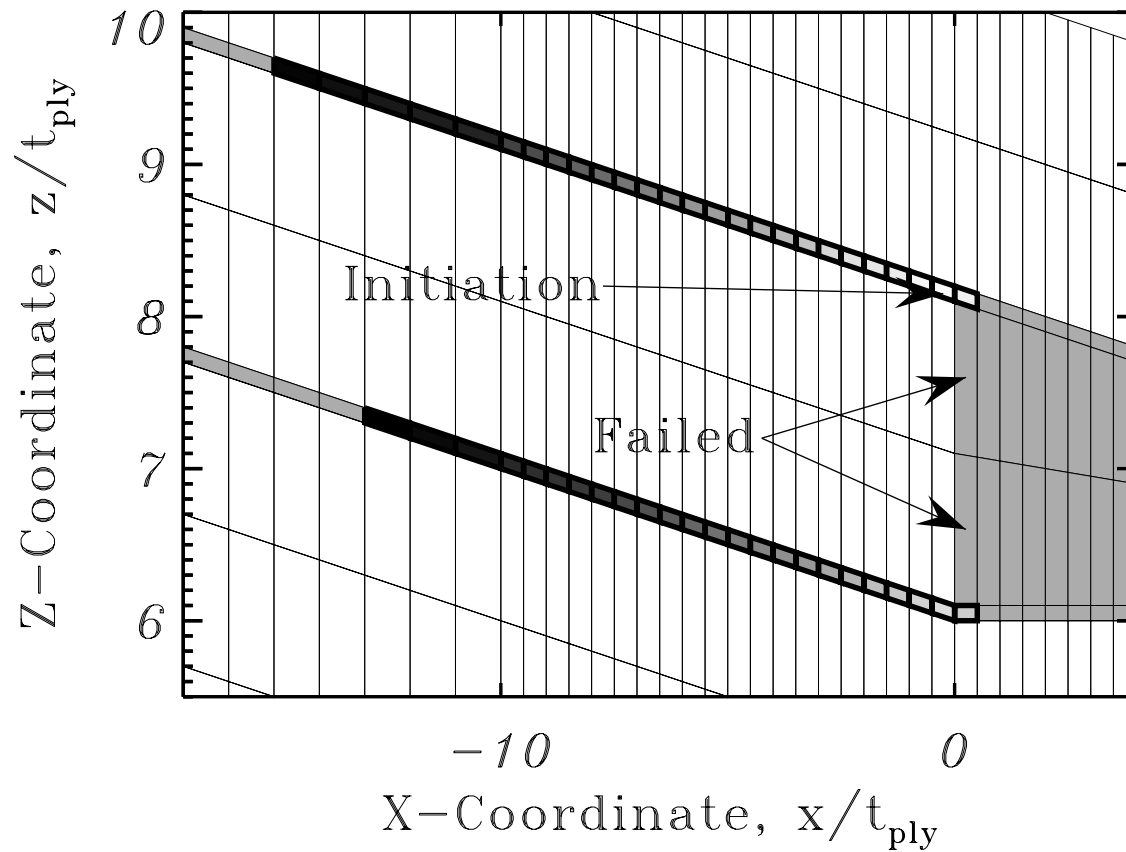


Figure 22 Delamination propagation for flawed overlapped-dispersed configuration

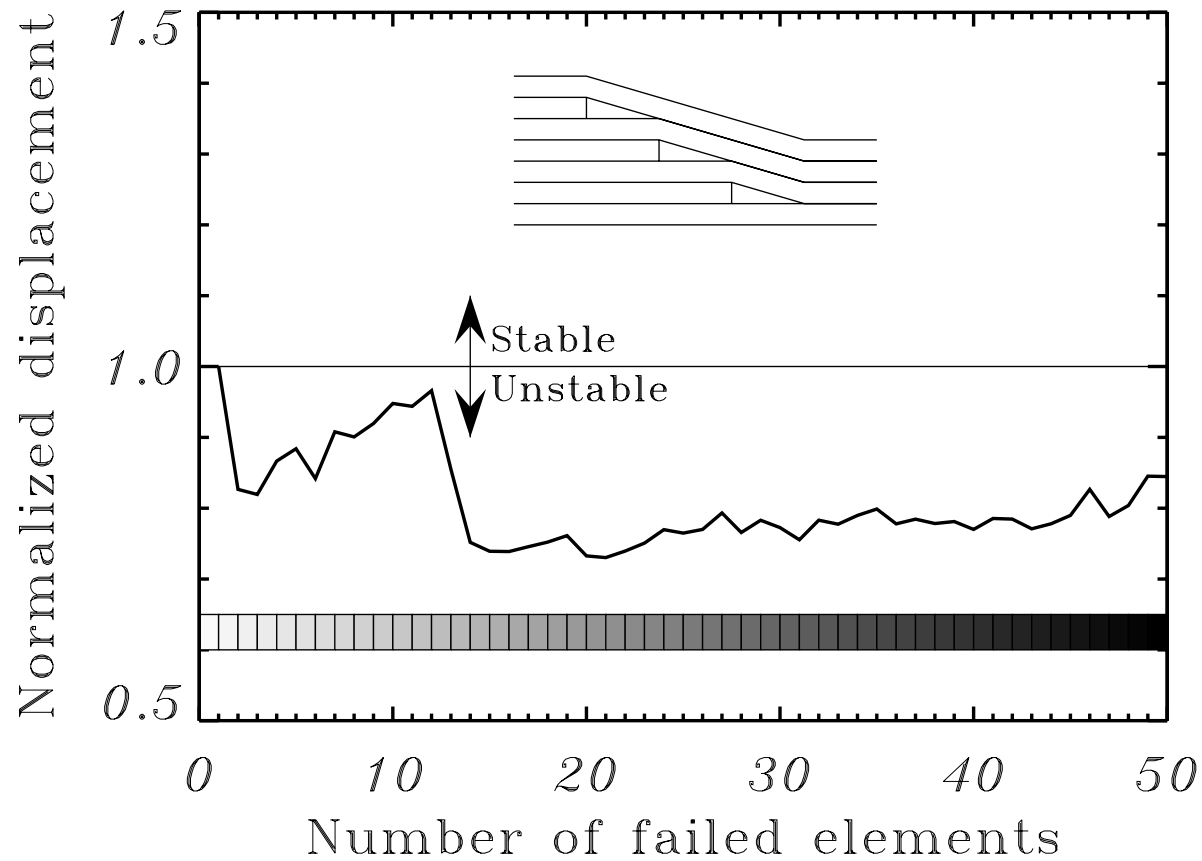


Figure 23 Normalized axial displacement versus number of failed elements for flawed staircased-dispersed configuration

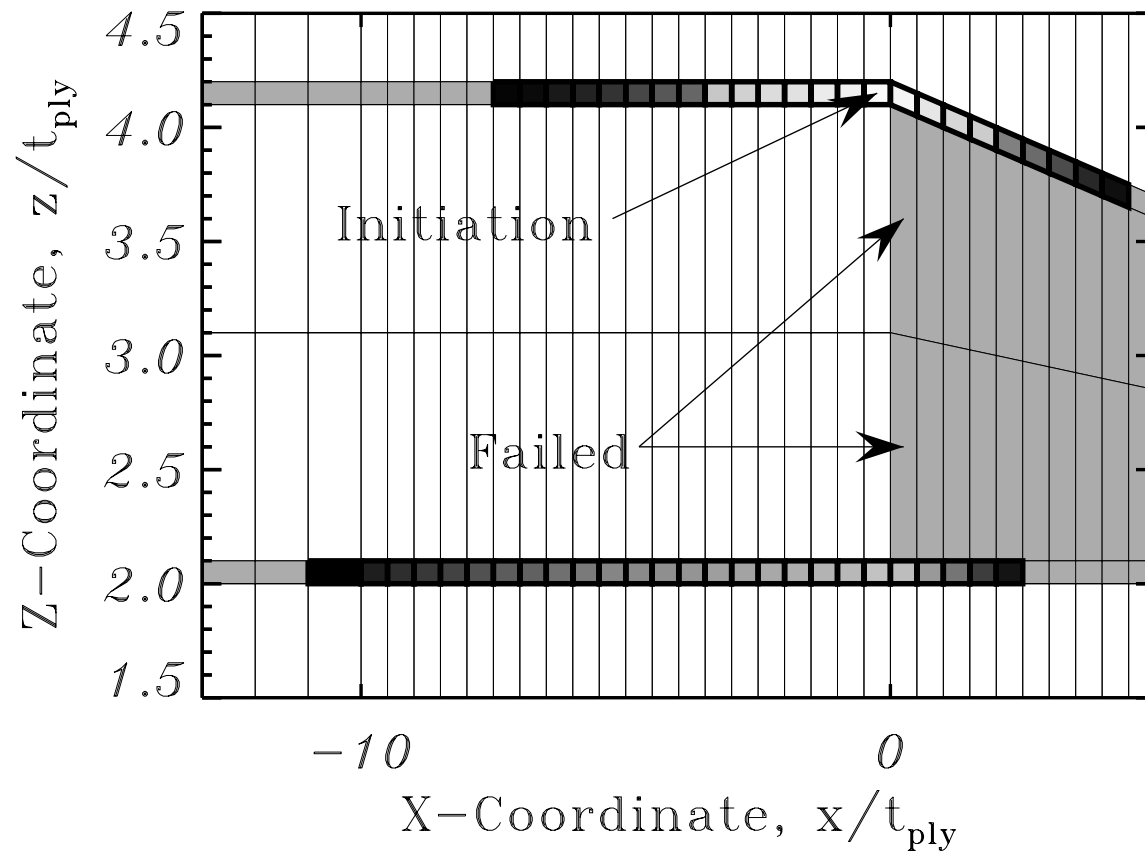


Figure 24 Delamination propagation for flawed staircased-dispersed configuration

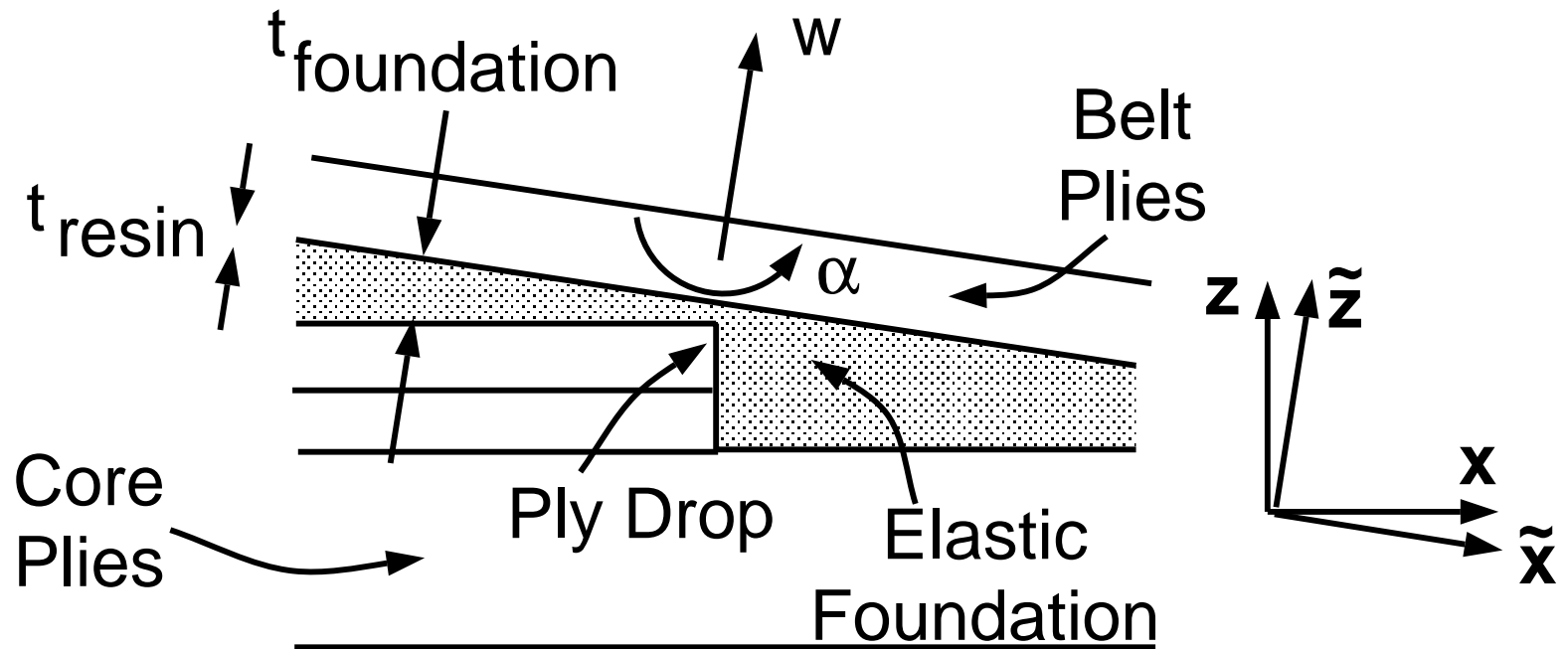


Figure 25 Schematic drawing of elastic foundation model

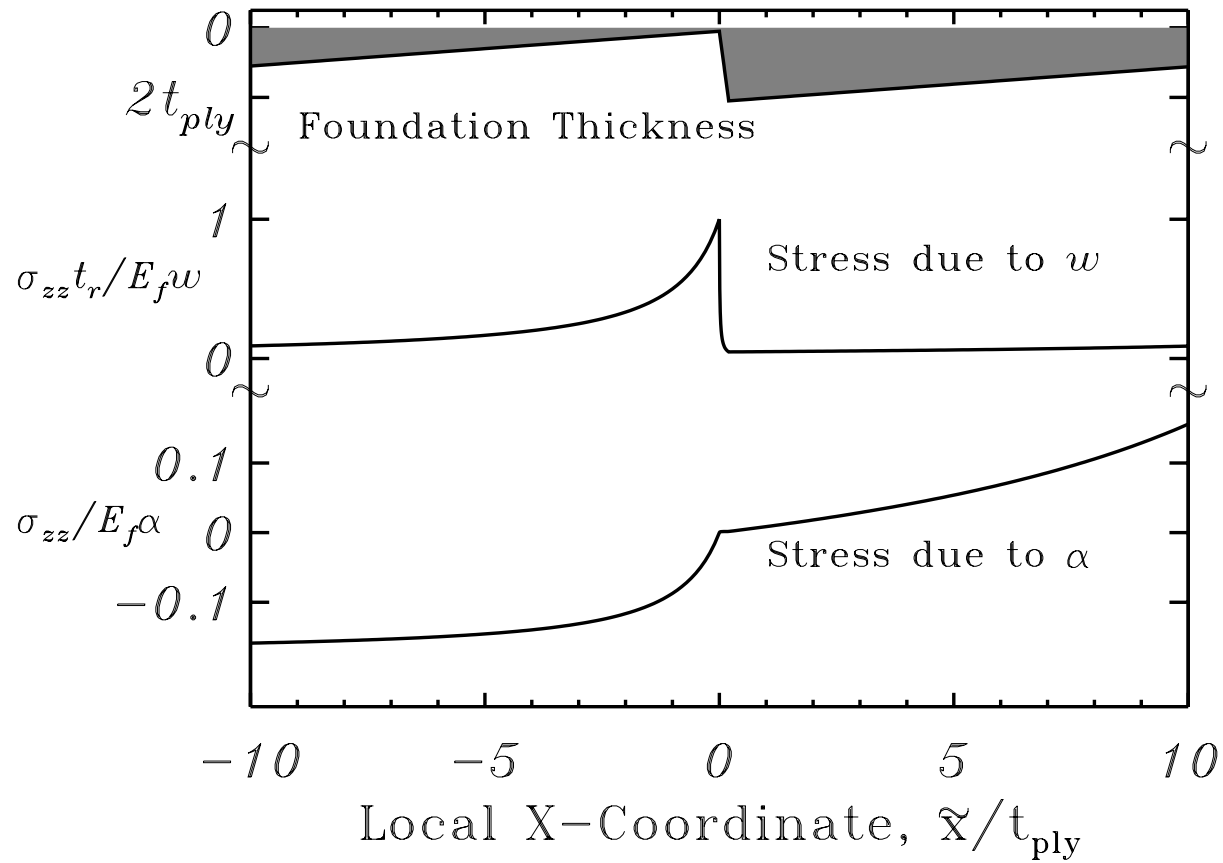


Figure 26 Stresses in foundation due to rotation and translation of rigid belt plies

Table 1 Material Properties [2]

Glass/Epoxy Unidirectional Tape	
Longitudinal Modulus	$E_L = 44.1 \text{ GPa}$
Transverse Modulus	$E_T = 12.4 \text{ GPa}$
In-plane Shear Modulus	$G_{LT} = 4.48 \text{ GPa}$
Out-of-plane Shear Modulus	$G_{TN} = 4.14 \text{ GPa}$
Major Poisson's Ratio	$\nu_{LT} = 0.29$
Out-of-plane Poisson's Ratio	$\nu_{TN} = 0.50$
Ply Thickness	$t_{ply} = 0.216 \text{ mm}$
Neat Resin	
Young's Modulus	$E = 3.9 \text{ GPa}$
Shear Modulus	$G = 1.0 \text{ GPa}$
Poisson's Ratio	$\nu = 0.37$
Interply Region Thickness	$t_{resin} = 0.0216 \text{ mm}$

Table 2 Maximum Interlaminar Stresses vs. Interply Thickness

Layup	$\frac{t_{resin}}{t_{ply}}$	Ply Drop		Taper Root	
		σ_{zz}	σ_{zx}	σ_{zz}	σ_{zx}
(KPa)					
[±45 ₂ /0 ₄] _s	0.10	54.1	121	17.2	11.4
	0.03	56.7	160	17.0	14.7
	0.01	57.0	193	17.1	24.9
[0 ₄ /±45 ₂] _s	0.10	45.4	105	34.2	52.4
	0.03	47.4	138	34.0	74.1
	0.01	48.0	165	33.8	117.0
[0 ₈] _s	0.10	81.4	214	23.6	44.6
	0.03	83.8	301	23.3	66.9
	0.01	84.0	385	23.3	108.8